

学位論文

Construction and Rotation Control
of a Metal-centered Circular Gear System

(金属を中心骨格とする環状ギアシステムの構築と回転運動制御)

平成27年12月博士(理学)申請

東京大学大学院理学系研究科

化学専攻

眞田 千馬

Abstract

Introduction

Visualization of chemical phenomena is a challenge in chemistry because the visual perception of molecular behaviors invisible to the naked eye could provide a new insight into molecular dynamics and chemical reactions. Although the development of optical microscopy has enabled us to obtain some images of molecular motions, the connection with a sub-micrometer-sized probe, which is several

hundreds times as large as the molecular machine, would denaturalize the original kinetics and dynamics. Alternatively, the correlation between motions and color changes of molecular machines holds the promise as a non-invasive estimation method except for light-sensitive molecules.

Self-assembled molecular architectures have great potential to achieve non-covalent regulation of molecular motions. A variety of molecular gearing systems, miniatures of macroscopic gears, have been exploited since 1980. Triptycene is one of the most often-used molecules as a three-bladed gear, and most of the gearing systems consist of two triptycene gear molecules.

In this study, I have designed a metallo-molecular gearing system, **1**, having a well-defined, self-assembled structure and two coordination sites for axial ligands that can regulate the rotating velocity of the triptycene gears depending on their bulkiness (Figure 1). 2,3,6,7,14,15-Hexamethyltriptycene was selected as an enlarged gear part featuring the rigid C_3 -symmetrical structure, which was expected to cause a large rotational barrier enough for easy analysis of the rotating velocity. A lantern-type dirhodium-tetracarboxylate complex was used as a metal-centered platform for four gears due to its easiness of synthesis and the pseudo- D_{4h} -symmetrical structure. The VT-NMR analysis revealed that the rotating velocities in solution were markedly affected by the donating properties of coordinating atoms and the bulkiness of axial ligands. Moreover, UV-vis absorption spectroscopy indicated that the solution colors, namely electronic states of the central dirhodium ions, are significantly affected by the steric factors of the axial ligands and therefore strongly correlated with the rotating velocity.

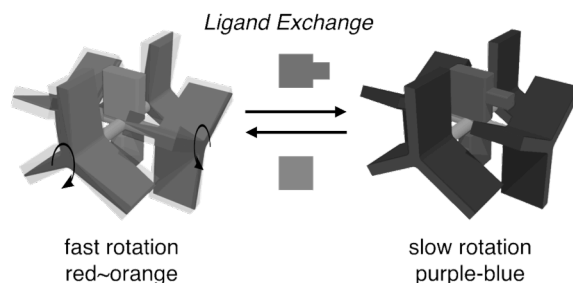


Figure 1. Schematic representation of rotational control of a molecular gearing system by axial ligand exchange.

Result and discussion

Synthesis. A molecular gearing system, **1**· L_2 , was prepared by mixing an ethanolic suspension of 2,3,6,7,14,15-hexamethyltriptycen-9-yl carboxylic acid, rhodium(III) chloride trihydrate and sodium carbonate. After purification by column chromatography and recrystallization from diethyl ether/ CH_2Cl_2 , a diethyl ether adduct **1**·(ether) $_2$ was obtained as

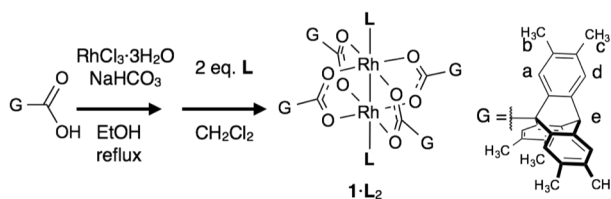


Figure 2. Synthesis of the molecular gearing system **1**· L_2 .

green crystals. The axial diethyl ether ligand could be replaced by several types of pyridines to form $1 \cdot L_2$ [$L = \text{py}$ (pyridine), **dmap** (*N,N*-dimethyl-4-aminopyridine), **min** (methyl isonicotinate), **mepy** (2-methylpyridine) and **etpy** (2-ethylpyridine)] by the addition of two equivalents of the corresponding pyridyl ligand in CH_2Cl_2 .

X-ray crystal structural analysis. Lantern-type structures of the molecular gearing systems $1 \cdot L_2$ with several types of axial ligands in the crystal state were analyzed by XRD measurement. Four gear-shaped triptyceny carboxylates were circularly arranged on the dirhodium center and meshed with each other in a zigzag conformation. Two axial ligands were bound to the dirhodium center along the Rh-Rh bond axis.

The structural parameters around the axial ligands are summarized in Table 1. The deviation among the Rh-Rh distances of the pyridyl ligand adducts fell within 0.01 Å, and the Rh-L distances were accurate

within 0.08 Å when the substituents at the 2-positions of the axial pyridyl ligands varied from proton to ethyl. In comparison, the Rh-Rh and Rh-L distances of the diethyl ether adduct were significantly shorter and longer, respectively. The bond angles Rh-Rh-N (axial ligand donor) reached 15° when the axial

ligand was the largest 2-ethylpyridine. These changing trends in the distances and angles suggest the steric repulsion around the axial ligands.

NMR study. Lantern-type structures of the molecular gearing systems in CDCl_3 were confirmed by NMR spectroscopy. The signals of methyl groups at the 2,7,14-positions of triptycene in each gearing system were up-field shifted compared with metal-free carboxylic acid. This result comes from the shielding effect from benzene rings of the adjacent triptycene, suggesting the meshing gear molecules stemmed from the lantern-type structure.

VT-NMR measurement at low temperatures showed 2:1 splitting of the signals of the blade parts of the gear molecules. This indicates that its zigzag conformation as observed in the crystal state is more stable than a tongue-and-groove conformation. The rotating velocity of each

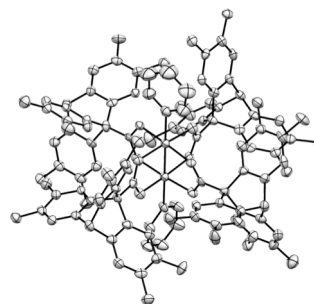


Figure 3. ORTEP representation of the X-ray structure of $1 \cdot (\text{py})_2$. Hydrogen atoms and solvent molecules are omitted for clarity.

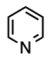
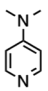
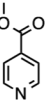
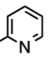
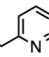
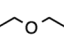
L						
Rh-Rh (Å)	2.40	2.41	2.40	2.41	2.41	2.37
Rh-L (Å)	2.25	2.22	2.23	2.28	2.30	2.31
Rh-Rh-L (°)	3.5	16.2	6.3	13.6	15.0	2.67

Table 1. Table for structural parameters of the molecular gearing systems with all axial ligands.

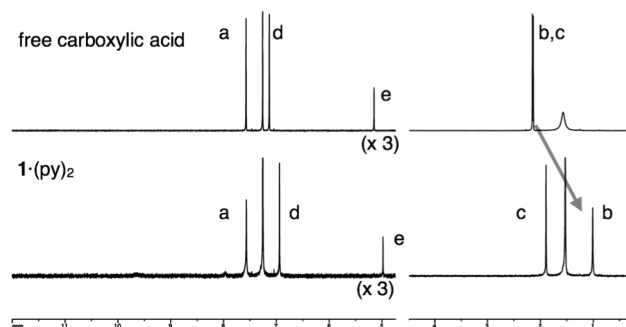


Figure 4. ^1H NMR spectra of free carboxylic acid and the molecular gearing system $1 \cdot (\text{py})_2$ at 300 K (500 MHz; CDCl_3 ; 0.1 mM)

complex at a given temperature was estimated by comparison with the dynamic NMR simulation. Eyring plots determined the activation parameters based on the temperature dependence of the rate constants for $\mathbf{1}\cdot(\mathbf{mepy})_2$, $\mathbf{1}\cdot(\mathbf{etpy})_2$ and $\mathbf{1}\cdot(\mathbf{ether})_2$: $\Delta H^\ddagger(\mathbf{mepy}) = 14.5 \text{ kcal mol}^{-1}$ and $\Delta S^\ddagger(\mathbf{mepy}) = 106 \text{ cal mol}^{-1} \text{ T}^{-1}$, $\Delta H^\ddagger(\mathbf{etpy}) = 17.92 \text{ kcal mol}^{-1}$ and $\Delta S^\ddagger(\mathbf{etpy}) = 116.7 \text{ cal mol}^{-1} \text{ T}^{-1}$, and $\Delta H^\ddagger(\mathbf{ether}) = 11.3 \text{ kcal mol}^{-1}$ and $\Delta S^\ddagger(\mathbf{ether}) = 99.3 \text{ cal mol}^{-1} \text{ T}^{-1}$, respectively. The rotating velocities and activation parameters of the gearing system with the other axial ligands could not be determined because no splitting behaviors were observed even at low temperatures. In comparison with the parameters of a pyridine adduct as a basis, the electronic modification of the pyridyl ligands (**dmap** and **min**) could not be very effective in controlling the rotating velocity. Moreover, bulky substituents at the 2-position of the pyridyl ligands (**mepy** and **etpy**) caused larger changes in the parameters than the type of donor atoms (nitrogen vs. oxygen).

UV-visible spectroscopy. The solution colors of the molecular gearing systems were analyzed by UV-visible spectroscopy. A broad absorption band around 500~600 nm was significantly shifted by changing the type of the axial ligands. The magnitude of the changes varied in the order of donor atoms (~80 nm), the bulkiness (~30 nm), and the electronic property (~10 nm) of the axial ligands. When the axial ligands were pyridine derivatives with a nitrogen donor atom, the bulkiness was the most influential factor affecting the color changes.

Conclusion

In conclusion, I have synthesized a molecular gearing system based on a lantern-type dirhodium complex. The lantern-type structures of molecular gearing systems in solution and in the crystal state were determined by NMR spectroscopy and X-ray analysis. The rotating velocities in solution, estimated by VT- ^1H NMR, were markedly-affected by the donating properties of coordinating atoms and the bulkiness of axial ligands, and the velocity changes were accompanied by the color changes of each solution. Such correlation would allow for the visualization of molecular motions.

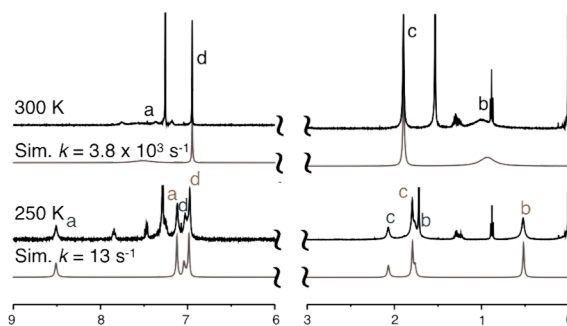


Figure 5. Measurements of the rate constants (k) for the 60° rotation process of a molecular gearing system $\mathbf{1}\cdot(\mathbf{mepy})_2$ were conducted by the dynamic ^1H NMR line-shape simulation (Sim).

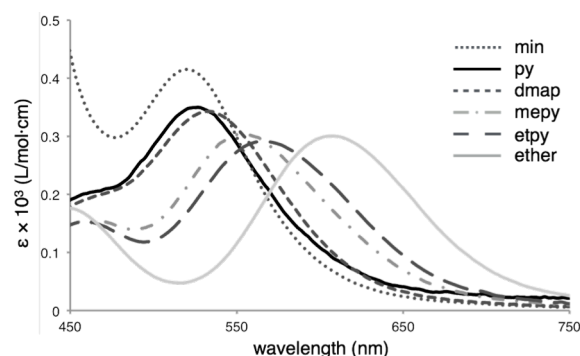


Figure 6. UV-vis spectra of molecular gear complexes (CHCl_3 solution: 20°C : 0.6 mM for **py**, 1 mM for others).

Abbreviations

Ac	acetyl
aq.	aqueous solution
ATP	adenosine triphosphate
Bu	butyl
ca.	centiare
Calcd	calculated
conc.	concentrated
DMSO	dimethyl sulfoxide
ESI	electrospray ionization
Et	ethyl
h	hour(s)
Hz	hertz
IPA	2-propanol
J	coupling constant
L	ligand
LRMS	low resolution mass spectrometry
M	metal ion
M	molar [mol/L]
Me	methyl
min	minute(s)
<i>m/z</i>	mass-to-charge ratio
<i>n</i>	normal
NMR	nuclear magnetic resonance
Ph	phenyl
ppm	parts per million
Py	pyridine
<i>t</i>	tertially
<i>T_c</i>	coalescence temperature
THF	tetrahydrofuran
THT	tetrahydrothiophene
TLC	thin layer chromatography
TMS	trimethylsilyl
TOF	time-of-flight
UV	ultraviolet
Vis	visible
VT	variable temperature

Contents

Abstract	— 1
Abbreviations	— 4
Contents	— 5
1. General Introduction	— 6
1-1. Chemistry of Molecular Rotors and Gear Systems	— 7
1-2. Triptycene	— 10
1-3. Metal Complexes in Molecular Machines	— 12
1-4. Aim of This Study	— 14
1-5. References	— 16
2. Rotation Control of a Metal-centered Circular Gear System	— 19
2-1. Introduction	— 20
2-2. Molecular Design of a Metal-centered Circular Gear System $1 \cdot L_2$	— 21
2-3. Synthesis and Crystal Structure of a Gear System $1 \cdot L_2$	— 22
2-4. Visible Absorption Spectroscopy of a Gear System $1 \cdot L_2$	— 25
2-5. NMR Study of a Gear System $1 \cdot L_2$	— 27
2-6. References	— 34
2-7. Experimental Section	— 35
2-8. References for Experimental Section	— 66
3. Conclusions and Perspectives	— 67
3-1. Conclusion	— 68
3-2. Perspectives	— 69
A List of Publication	— 71
Acknowledgement	— 72

1. General Introduction

1-1. Chemistry of Molecular Rotors and Gear Systems

In 1959, Feynman (Nobel Prize in Physics in 1965) first discussed a concept of nanomachine in his lecture *There's Plenty of Room at the Bottom*¹. He considered the possibility and benefit of direct manipulation of atoms with step-by-step miniaturized tools, "*I manufacture quarter-size tools; and I make, at the one-quarter scale, still another set of hands again relatively one-quarter size! This is one-sixteenth size, from my point of view.*" Although his top-down process could not reach the atomic scale due to the change of predominant forces in the nanoscale world, it is now considered that a bottom-up process as seen in molecular machines can achieve his dream. Molecular machines are defined as molecules whose mechanical motion can be controlled by artificial manipulations. For the last several decades, a great number of researchers have developed a variety of molecular machines². In 2016, the Nobel Prize in Chemistry was awarded jointly to Sauvage³, Stoddart⁴ and Feringa⁵ "*for the design and synthesis of molecular machines*"⁶.

In living things, biological molecular machines work to maintain their lives in a cooperative manner. ATP synthase produces energy source with unidirectional rotation, myosin is essential for locomotion of animals, and kinesin and dynein transport cellular cargo. Recent researches have clarified that biological molecular machines take full advantages of uncertainty, which is excluded as a noise from macroscopic machines. For example, myosin shows a few steps on an actin filament against an ATP molecule⁷. Although a biological molecular machine is a successful nanomachine, an artificial molecular machine that mimics a straightforward macroscopic machine would have a potential to achieve nanomachines.

A gear has been extensively used as a fundamental component in artificial macroscopic

machines that conducts propagation of rotation, control of direction and synchronization of motions. Recent researches have revealed that a gear function is utilized in nymphs of the flightless planthopper insect *Issus*⁸ and marine bacterium MO-1⁹, which encourages our use of gears for artificial macroscopic machines. Understanding nano-scaled gears would help us to design and control motions of artificial molecular machines. When multiple artificial molecular machines are connected with each other in a well-defined manner through a nano-scaled gear system, the motions would be transformed and synchronized to achieve practical functions.

A molecular gear system was first reported by Iwamura¹⁰ and Mislow¹¹, independently (Figure 1-1-1a). Their molecular gear systems were composed of two triptycene gear molecules connected through a methylene or an ether group on the bridgehead positions. The authors theoretically determined 1-2 kcal mol⁻¹ for energy barrier of engaged rotation, and experimentally 32-45 kcal mol⁻¹ for energy barrier of slippage rotation. The energy barrier of engaged rotation is generally low causing too fast rotation to observe. Mislow's gear system, in which triptycene gears were substituted to increase steric repulsion, is only a gear system in which energy barrier of engaged rotation of triptycene gears was determined experimentally.

A variety of linker structures with different distance and angle between two triptycene gears^{12,13} have been reported for tuning the energy barriers of engaged and slippage rotational motions (Figure 1-1-1b-g). It was notable that Kira was successful in switching engaged and disengaged rotational motions of two triptycene gears which were connected through a difluorosilylene group by a fluoride anion, and the gear system showed a clutch function (Figure 1-1-1g)¹³. This system is considered as a molecular machine, in the strict sense, because of its controllable motion by artificial manipulation. Molecular gear systems using pentiptycene gears¹⁴ and porphyrin gears¹⁵ as

four-blade gears were also reported. Pentiptycene gears were not prospective because of the low energy barrier for slippage rotation ($< 6 \text{ kcal mol}^{-1}$).

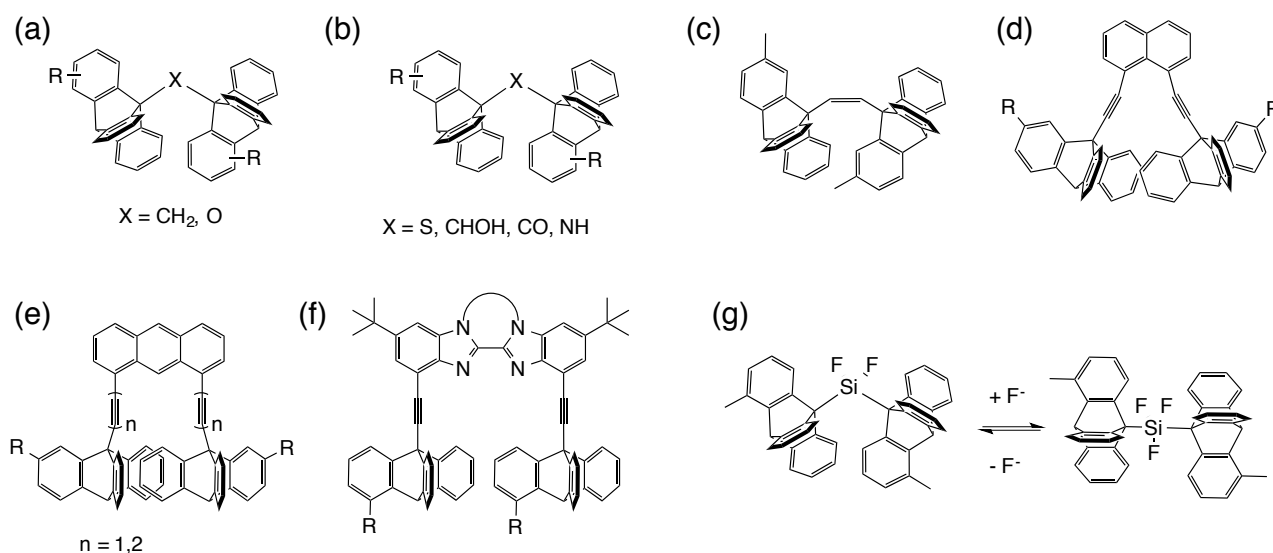


Figure 1-1-1. Molecular gear systems composed of two triptycene gears connected through various linkers

Considering effects of the distance and angle between two gears on the engaged rotation is important for designing molecular gear systems as in the case with macroscopic machines. Multiple gear arrangement is also important to develop higher molecular functions as a number of excellent engaged gear systems have been used for macroscopic machines. However, only a few molecular gear systems composed of three gears^{10,11,14} have been reported. Iwamura reported a linearly arranged gear system (Figure 1-1-2a). Mislow reported circularly arranged three gear systems (Figure 1-1-2b,c). The circularly arranged gear systems cannot rotate without slippage rotational motion because a gear counterrotates to the adjacent gear. Thus, few systems composed of more than three gears have been developed so far.

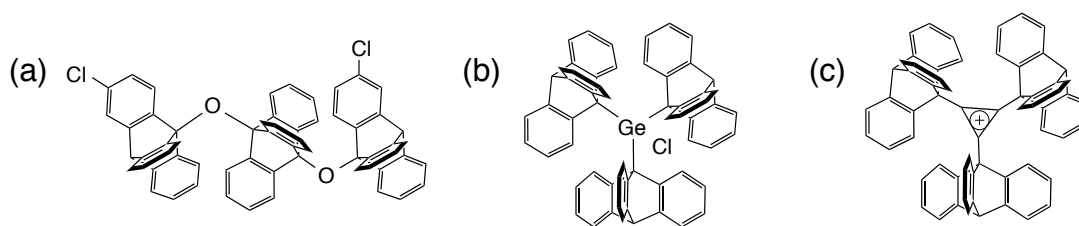


Figure 1-1-2. Molecular gear systems composed of three triptycene gears connected through various linkers

1-2. Triptycene

Triptycene is a D_{3h} -symmetrical rigid molecule, which was firstly synthesized by Bartlet in 1942¹⁶. After the discovery of a simplified synthetic method, which is Diels-Alder reaction of anthracene with benzyne¹⁷, its structural features have been more frequently utilized for frameworks of molecular rotors.

Triptycene is a useful component for molecular rotors due to its easy observation of the rotation (Figure 1-2-1). When a C_2 -symmetrical component like a benzene ring is connected to the bridgehead position of triptycene, three blades are chemically equivalent under fast rotation but inequivalent under slow rotation. The observation of a translation between these two different states enables us to estimate the rotational velocity. It is important that both fast and slow rotations lie in the observable range of the measuring method. It should be noted that we could observe only a one-third rotation, and could not distinguish unidirectional rotation and oscillation.

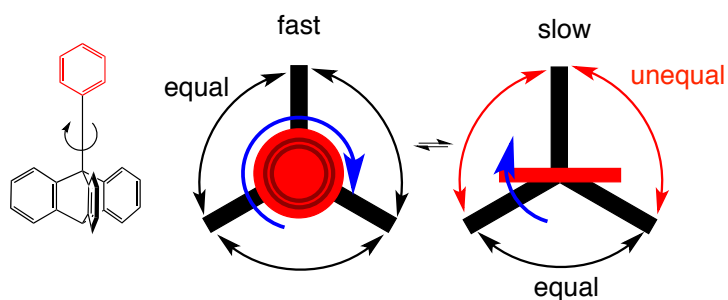


Figure 1-2-1. Observation of rotation using triptycene

Triptycene is often used not only for a molecular gear system as described above, but also for other types of molecular machines (Figure 1-2-2). Kelly reported a molecular rotary motor which can unidirectionally rotate by 120° using urethane formation and hydrolysis¹⁸. And his group further reported a molecular brake in which the rotational rate is decreased due to the steric repulsion of a pyridyl group fixed by complexation with an Hg^{2+} cation¹⁹. McGlinchey also developed a molecular brake in which the rate is decreased by haptotropic rearrangement²⁰.

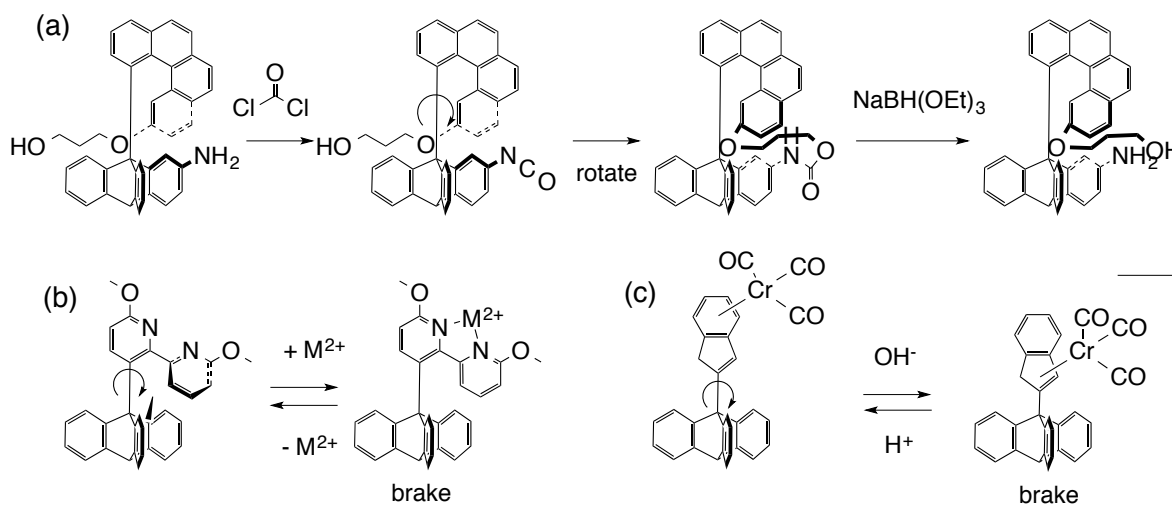


Figure 1-2-2. Molecular motor and brakes using triptycene framework

1-3. Metal Complexes in Molecular Machines

A metal complex usually consists of a central metal atom or ion and ligands. The type and oxidation number of the metal ion affect the character of the coordination bonds between the metal and ligands. Control of lability of coordination bonds has been utilized for switching motions in molecular machines. Sauvage reported a [2]catenate rotor in which the redox reaction of the central copper ion caused exchange of the [2]catenate ligands (Figure 1-3-1a)²¹. They also reported a [2]rotaxane motor with a similar mechanism (Figure 1-3-1b)²².

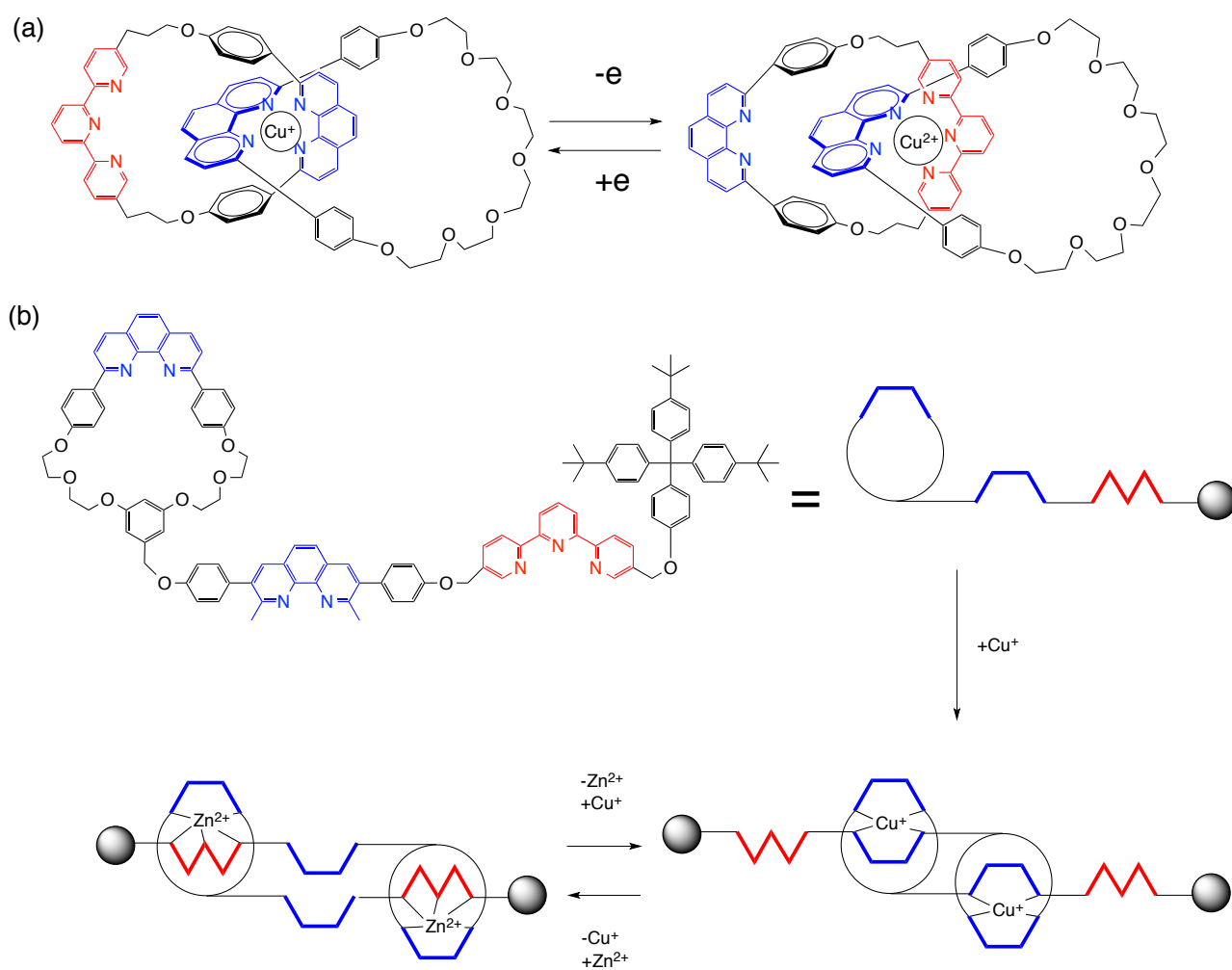


Figure 1-3-1. Molecular rotor and motor using metal complexes

Metal complexes are also utilized for molecular gear systems as a linker. Richards reported a gear system composed of a three-blade and a four-blade gears²³ which were connected through a cobalt ion (Figure 1-3-2a). This was the first example of the use of cyclopentadienyl scaffold as a metal-mediated four-blade gear. Shinkai has developed porphyrin gear systems based on a double-decker complex (Figure 1-3-2b)²⁴. The engaged rotation of the complexes was controlled by the allonomous changes in the coordination mode of the double-decker complex. These systems are also considered as distinct molecular machines. Kobayashi has developed porphyrin gear systems on a cavitand scaffold (Figure 1-3-2c)²⁵. The engaged rotation of the complexes was analyzed theoretically and experimentally.

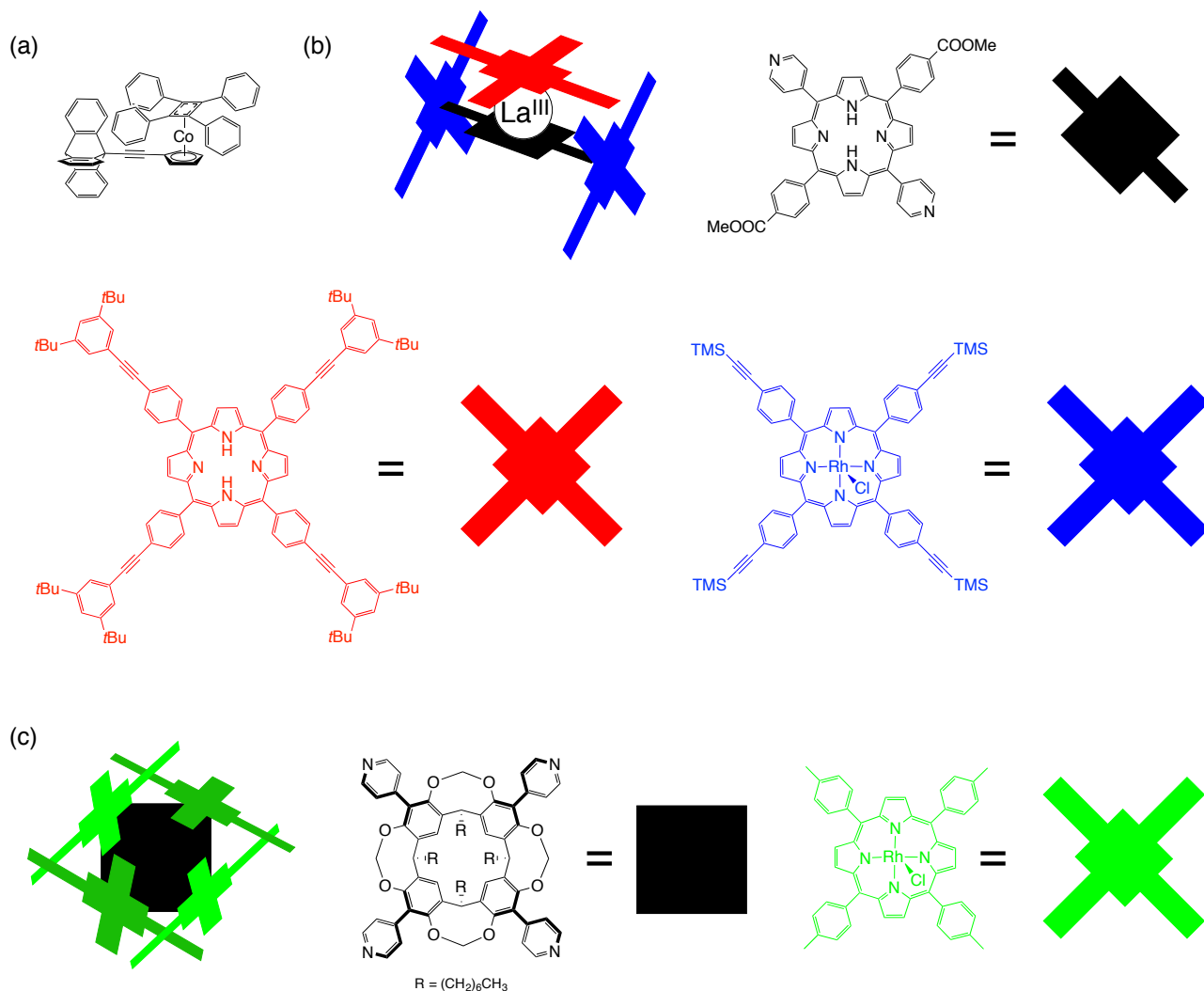


Figure 1-3-2. Metal-mediated molecular gear systems

1-4. Aim of This Study

As described above, a molecular gear system is considered as an important component of artificial molecular machines. Although the development of arrangement methods for multiple gears and the analytical study on their effects on the engaged rotational motions are important issues in this field, the mechanistic details have yet to be revealed. In this study, I chose a metal complex as a central stator to arrange multiple triptycene gears in an easily-controllable way. I also

chose a substituted triptycene gear to increase the energy barrier of the engaged rotation.

A dinuclear lantern-type complex was used in this study, whose D_4 -symmetric structure enables arrangement of four gears circularly on the central dinuclear metal-metal bond. I found that the enlarged triptycene gear, 2,3,6,7,14,15-hexamethyltriptycen-9-yl groups, incorporated into the structure provided useful information to analyze the rotational motions. The axial ligands of the lantern-type complex affected the engaged rotation, and this system can be considered as a distinct molecular machine (Figure 1-4-1).

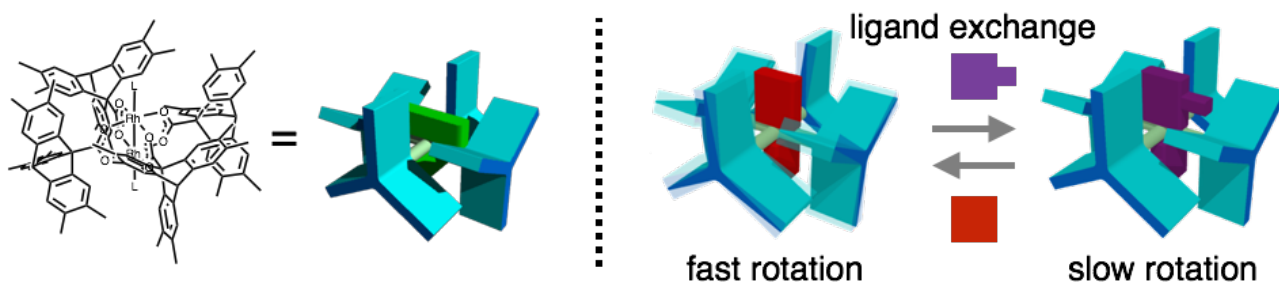


Figure 1-4-1. Molecular design of a molecular gear system based on a lantern-type complex

This thesis consists of three chapters as follows: In chapter 1, the background of molecular gear systems and the design concept of metal-based gear systems are described. Chapter 2 describes the synthesis and properties of a molecular gear system based on a lantern-type complex, and its rotational behaviors with a variety of axial ligands. Chapter 3 includes conclusion of this study and perspectives of molecular gear systems based on a metal complex.

1-5. References

1. R. P. Feynman, *Eng. Sci.* **1960**, *23*, 22–36.
2. (a) R. Ballardini, V. Balzani, A. Credi, M. T. Gandolfi, M. Venturi, *Acc. Chem. Res.* **2001**, *34*, 445–455. (b) B. L. Feringa, *Acc. Chem. Res.* **2001**, *34*, 504–513. (c) T. R. Kelly, *Acc. Chem. Res.* **2001**, *34*, 514–522. (d) W. R. Browne, B. L. Feringa, *Nat. Nanotechnol.* **2006**, *1*, 25–35. (e) B. Champin, P. Mobian, J.-P. Sauvage, *Chem. Soc. Rev.* **2007**, *36*, 358–366. (f) E. R. Kay, D. A. Leigh, *Angew. Chem. Int. Ed.* **2015**, *54*, 10080–10088.
3. (a) C. O. Dietrich-Buchecker, J.-P. Sauvage, J.-P. Kintzinger, *Tetrahedron Lett.* **1983**, *24*, 5095–5098. (b) C. O. Dietrich-Buchecker, P. A. Marnot, J.-P. Sauvage, *Tetrahedron Lett.* **1982**, *23*, 5291–5294.
4. (a) P. L. Anelli, N. Spencer, J. F. Stoddart, *J. Am. Chem. Soc.* **1991**, *113*, 5131–5133. (b) B. Odell, M. V. Reddington, A. M. Z. Slawin, N. Spencer, J. F. Stoddart, D. J. Williams, *Angew. Chem. Int. Ed.* **1988**, *27*, 1547–1550.
5. N. Koumura, R. W. J. Zijlstra, R. A. van Delden, N. Harada, B. L. Feringa, *Nature* **1999**, *401*, 152–155.
6. “The Nobel Prize in Chemistry 2016”. *Nobelprize.org*. Nobel Media AB 2014. Web. 20 May 2017. <http://www.nobelprize.org/nobel_prizes/chemistry/laureates/2016/>
7. T. Yanagida, T. Arata, F. Oosawa, *Nature* **1985**, *316*, 366–369.
8. M. Burrows, G. Sutton, *Science* **2013**, *341*, 1254–1256.
9. J. Ruan, T. Kato, C.-L. Santini, T. Miyata, A. Kawamoto, W.-J. Zhang, A. Bernadac, L.-F. Wu, K. Namba, *Proc. Natl. Acad. Sci.* **2012**, *109*, 20643–20648.

10. (a) Y. Kawada, H. Iwamura, *J. Am. Chem. Soc.* **1981**, *103*, 958–960. (b) Y. Kawada, H. Iwamura, *Tetrahedron Lett.* **1981**, *22*, 1533–1536.
11. (a) W. D. Hounshell, C. A. Johnson, A. Guenzi, F. Cozzi, K. Mislow, *Proc. Natl. Acad. Sci.* **1980**, *77*, 6961–6964. (b) F. Cozzi, A. Genzi, C. A. Johnson, K. Mislow, *J. Am. Chem. Soc.* **1981**, *103*, 957–958. (c) C. A. Johnson, A. Genzi, K. Mislow, *J. Am. Chem. Soc.* **1981**, *103*, 6240–6242. (d) A. Genzi, C. A. Johnson, F. Cozzi, *J. Am. Chem. Soc.* **1983**, *105*, 1438–1448.
12. -S-: (a) Y. Kawada, J. Ishikawa, H. Yamazaki, G. Koga, S. Murata, H. Iwamura, *Tetrahedron Lett.* **1987**, *28*, 445–448. -CHOH-: ref 8d. -CO-: (b) C. A. Johnson, A. Genzi, R. B. Jr. Nachbar, J. F. Bount, O. Wennerstrom, K. Mislow, *J. Am. Chem. Soc.* **1982**, *104*, 5163–5168. -NH-: (c) Y. Kawada, H. Yamazaki, G. Koga, S. Murata, H. Iwamura, *J. Org. Chem.* **1986**, *51*, 1472–1477. -CH=CH-: (d) Y. Kawada, H. Sasaki, M. Oguri, G. Koga, S. Murata, *Tetrahedron Lett.* **1994**, *35*, 139–142. Others: (e) S. Toyota, T. Shimizu, T. Iwanaga, K. Wakabayashi, *Chem. Lett.* **2011**, *40*, 312–314. (f) D. K. Frantz, A. Linden, K. K. Baldrige, J. S. Siegel, *J. Am. Chem. Soc.* **2012**, *134*, 1528–1535.
13. W. Setaka, T. Nirengi, C. Kabuto, M. Kira, *J. Am. Chem. Soc.* **2008**, *130*, 15762–15763.
14. C.-Y. Kao, Y.-T. Hsu, H.-F. Lu, I. Chao, S.-L. Huang, Y.-C. Lin, W.-T. Sun, J.-S. Yang, *J. Org. Chem.* **2011**, *76*, 5782–5792.
15. (a) S. Ogi, T. Ikeda, R. Wakabayashi, S. Shinkai, M. Takeuchi, *Chem. Eur. J.* **2010**, *16*, 8285–8290. (b) S. Ogi, T. Ikeda, R. Wakabayashi, S. Shinkai, M. Takeuchi, *Eur. J. Org. Chem.* **2011**, 1831–1836.
16. P. D. Bartlett, M. J. Ryan, S. G. Cohen, *J. Am. Chem. Soc.* **1942**, *64*, 2649–2653.
17. G. Wittig, R. Ludwig, *Angew. Chem.* **1956**, *68*, 40.

18. T. R. Kelly, H. D. Silva, R. A. Silva, *Nature* **1999**, *401*, 150–152.
19. T. R. Kelly, M. C. Bowyer, K. V. Bhaskar, D. Bebbington, A. Garcia, F. Lang, M. H. Kim, M. P. Jette, *J. Am. Chem. Soc.* **1994**, *116*, 3657–3658.
20. K. Nikitin, H. Muller-Bunz, Y. Ortin, M. J. McGlinchey, *Chem. Eur. J.* **2009**, *15*, 1836–1843.
21. (a) A. Livoreil, C. O. Dietrich-Buchecker, J.-P. Sauvage, *J. Am. Chem. Soc.* **1994**, *116*, 9399–9400. (b) A. Livorel, J.-P. Sauvage, N. Armaroli, V. Balzani, L. Flamigni, B. Ventura, *J. Am. Chem. Soc.* **1997**, *119*, 12114–12124. (c) F. Baumann, A. Livoreil, W. Kaim, J.-P. Sauvage, *Chem. Commun.* **1997**, 35–36.
22. (a) P. Gaviña, J.-P. Sauvage, *Tetrahedron Lett.* **1997**, *38*, 3521–3524. (b) N. Armaroli, V. Balzani, J.-P. Sauvage, B. Ventura, *J. Am. Chem. Soc.* **1999**, *121*, 4397–4408.
23. A. M. Stevens, C. J. Richards, *Tetrahedron Lett.* **1997**, *38*, 7805–7808.
24. (a) S. Ogi, T. Ikeda, R. Wakabayashi, S. Shinkai, M. Takeuchi, *Chem. Eur. J.* **2010**, *16*, 8285–8290. (b) S. Ogi, T. Ikeda, R. Wakabayashi, S. Shinkai, M. Takeuchi, *Eur. J. Org. Chem.* **2011**, 1831–1836.
25. M. Nakamura, K. Kishimoto, Y. Kobori, T. Abe, K. Yoza, K. Kobayashi, *J. Am. Chem. Soc.* **2016**, *138*, 12564–12577.

2. Rotation Control of a Metal-centered Circular Gear System

2-1. Introduction

A lantern-type complex, which is also called a paddlewheel complex, has a structure in which four bidentate ligands, usually carboxylates, are coordinated with two metal ions as shown in Figure 2-1-1a. Since the first structure was reported for copper(II) acetate by van Niekerk and Schoening in 1953¹, a number of examples have been reported which combined various bridging ligands with metal ions. The d-orbitals of two late transition metal ions overlap with each other, causing an unusual electronic structure of a lantern-type complex. Most of lantern-type complexes represent metal-metal bonding depending on the number of d electrons, which have significant influence on the contribution of bonding and antibonding orbitals to the bond order as shown in Figure 2-1-1b. The equatorial position of the dinuclear metal center is coordinated by bidentate bridging ligands, and the two axial positions are usually coordinated by a monodentate ligand for each. With multi-monodentate ligands, lantern-type complexes can be linked. In this unique structure, the type of axial ligands possibly becomes an important factor to determine the electronic property of the dinuclear metal center.

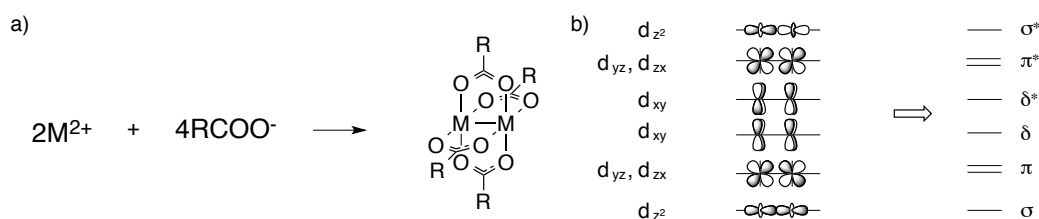


Figure 2-1-1. a) A general reaction scheme and b) electronic structure of a lantern-type complex

A lantern-type dinuclear rhodium(II) complex, which was first reported by Chernyaev in 1960², has a single metal-metal bond due to occupied δ^* and π^* orbitals and an unoccupied σ^* orbital. The energy level of the σ^* orbital is sensitively affected by the orbitals of the axial ligands. The visible

absorption depends on the energy gap of π^* - σ^* transition of the dinuclear metal center, which leads to the color changes depending on the type of axial ligands. The theoretical study of the electronic structures, the application to anti-tumor treatment and catalysis for various reactions such as decomposition reaction of azo compounds have received attention in recent years.

Triptycene can be regarded as a bulky and tightly-meshed substituent and a few examples of lantern-type complexes with triptycene have been so far reported. Lippard reported a lantern-type iron complex protected by bulky triptycene, which gained remarkable stability to water³. Rieger used triptycene-9,10-dicarboxylate as a bridging ligand for metal-organic framework, and revealed the stabilization by π - π and CH- π interactions between triptycenes⁴. Noels used a lantern-type dinuclear rhodium complex for the investigation of the steric effect on the selectivity for C-H insertion reaction of decomposed diazo compounds⁵. However, none of these studies has investigated the dynamic behavior of the complexes in solution or in the solid state.

2-2. Molecular Design of a Metal-centered Circular Gear System 1·L₂

A lantern-type complex has favorable characters as a scaffold for regular gear arrangement for engaged rotation. In a variety of metals used for a lantern-type dinuclear center, I chose a dinuclear Rh(II) complex as a stator of gear systems, which has easy handiness under ambient condition due to the high stability in air and moisture. And proper inertness for the bridging ligand exchange gives stable observation at room temperature and ligand exchange in refluxing solvents.

The axial ligands **L** of a lantern-type complex was supposed to act as a factor to control the engaged rotation due to the steric and electronic effects. Axial ligand exchange easily takes place in

solution, and this would enable post-tuning of the engaged rotation of the gear system.

A triptycene gear was modified for easy observation of the rotation. Expanding the length of the blade of gears would enhance the rotational barrier due to the tight steric interactions. Methyl groups were chosen as the substituents at appropriate positions of the blade part because of their extremely low coordination ability to the dinuclear rhodium center and of synthetic easiness. The 2-, 3-, 6-, 7-, 14-, and 15-positions of triptycene were methylated reduce the number of structural isomers of 9-bromotriptycene, which was a precursor of the corresponding carboxylic acid, because triptycene derivatives are mostly synthesized by Diels-Alder reaction of the corresponding anthracene and benzyne.

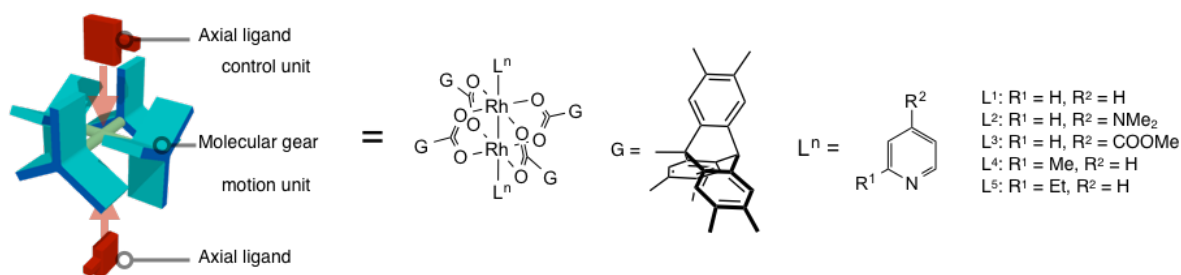


Figure 2-2-1. Schematic illustration and chemical structure of a molecular gear system $\mathbf{1} \cdot \mathbf{L}_2$

2-3. Synthesis and Crystal Structure of a Gear System $\mathbf{1} \cdot \mathbf{L}_2$

The designed gear system was synthesized according to a little modified method for $Rh_2(CH_3CO_2)_4(H_2O)_2$ and isolated as an ether adduct $\mathbf{1} \cdot (\text{ether})_2$, in which the axial ligands are diethyl ether. 9-Bromo-2,3,6,7,14,15-hexamethyltriptycene was synthesized by the Diels-Alder reaction of 9-bromo-2,3,6,7-tetramethylantracene with substituted benzyne derived from 4,5-dimethylantranilic acid, and then lithiated by *t*-butyllithium followed by carboxylation with

carbon dioxide. The obtained carboxylic acid was reacted with $\text{RhCl}_3 \cdot 3\text{H}_2\text{O}$ in refluxing ethanol in the presence of sodium hydrogen carbonate for 24 h to afford a mixture of lantern-type dinuclear rhodium complexes. After purification by column chromatography and recrystallization by slow evaporation from a mixture of dichloromethane and diethyl ether, diethyl ether adduct $\mathbf{1} \cdot (\text{ether})_2$ was obtained as green crystals in 48% yield. ESI-MS analysis was carried out after addition of a sodium iodide solution to a solution of $\mathbf{1} \cdot (\text{ether})_2$ to detect a species as $\mathbf{1} \cdot \text{I}^-$ in which each axial diethyl ether ligand was replaced by an iodide ion.

The two axial diethyl ether ligands were replaced by several types of pyridine ligands to form $\mathbf{1} \cdot \text{L}_2$ [$\text{L} = \text{py}$ (pyridine), *dmap* (*N,N*-dimethyl-4-aminopyridine), *min* (methyl isonicotinate), *mepy* (2-methylpyridine), and *etpy* (2-ethylpyridine)] after addition of two equivalents of the corresponding pyridine derivatives in dichloromethane. The crystals of these adducts were obtained by the corresponding method (see 2-7 Experimental).

X-ray crystal structure analyses were carried out for all the six adducts. An X-ray crystal structure of the diethyl ether adduct $\mathbf{1} \cdot (\text{ether})_2$ is shown in Figure 2-3-1. The dinuclear rhodium core of the lantern-type complex was surrounded by four carboxylate gears meshing with each other, and its dinuclear rhodium center was sandwiched between two axial ether ligands along the Rh-Rh bond axis.

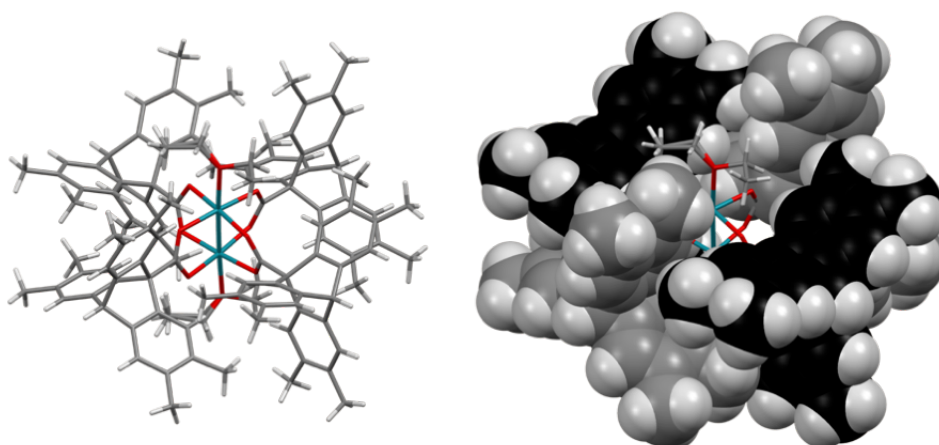
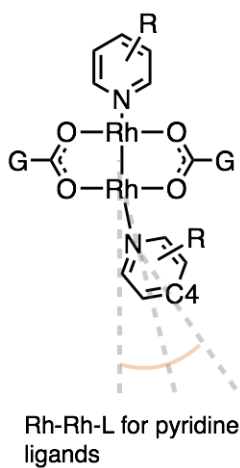


Figure 2-3-1. Crystal structure of a molecular gear system $1 \cdot (\text{ether})_2$

The structural parameters around the axial ligands are summarized in Table 2-3-2. The deviation among Rh–Rh distances fell in 0.01 Å, and the Rh–L distances extended 0.08 Å according to the change of the substituents from proton to ethyl at the 2-positions of the axial ligands. The bending angles of the axial ligands from the Rh–Rh bond axis showed smaller values, 3.5° and 6.3°, in $1 \cdot (\text{py})_2$ and $1 \cdot (\text{min})_2$, respectively. On the other hand, the bending angle showed larger values, 16.2°, 13.6°, and 15.0°, in $1 \cdot (\text{dmap})_2$, $1 \cdot (\text{mepy})_2$, and $1 \cdot (\text{etpy})_2$, respectively. In $1 \cdot (\text{ether})_2$, the Rh–Rh distance was shorter, and the Rh–L distance was longer than those of the complexes with pyridine ligands.

Table 2-3-2. Structural parameters of molecular gear systems $1 \cdot L_2$

L	py	dmap	min	mepy	etpy	ether
Rh–Rh (Å)	2.40	2.41	2.40	2.41	2.41	2.37
Rh–O (Å)	2.03	2.04	2.04	2.04	2.03	2.04
Rh–L (Å)	2.25	2.22	2.23	2.28	2.30	2.31
Rh–Rh–L (°)	3.6	16.3	6.3	13.6	16.0	2.7



X-ray crystal structural analyses indicated the steric repulsion between the lantern-type complex and the substituents at the 2-positions of the pyridine ligands. The bulkier the axial ligands became, the longer the Rh-L distances became and the larger the bending angle became in the direction so as to reduce the steric repulsion with the substituents. In $\mathbf{1} \cdot (\text{dmap})_2$, the bending angle showed a large value of 16.3° due to the intermolecular $\pi-\pi$ interaction between the axial ligands of two complexes in the crystal packing as shown in Figure 2-3-3.

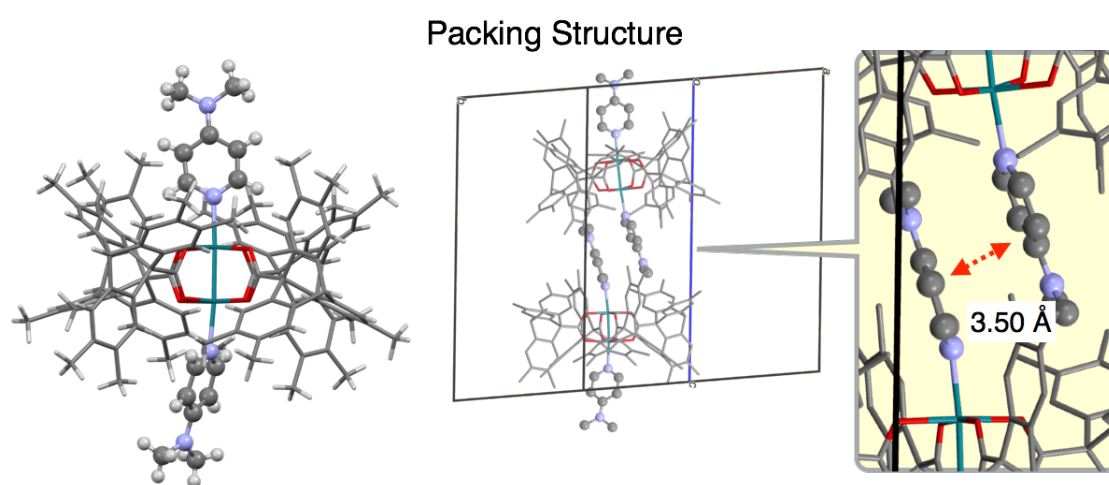


Figure 2-3-3. Crystal packing of a molecular gear systems $\mathbf{1} \cdot (\text{dmap})_2$

2-4. Visible Absorption Spectroscopy of a Gear System $\mathbf{1} \cdot \mathbf{L}_2$

The electronic structures of lantern-type complexes were then examined by visible absorption spectroscopy. Visible absorption spectral data of the complexes $\mathbf{1} \cdot \mathbf{L}_2$ in CHCl_3 are given in Figure 2-4-1 to compare the effects of the axial ligands on their electronic states. The effects of the type of carboxylates bridging Rh-Rh on the electronic states have been studied in detail. It is well known for $\text{Rh}_2(\text{RCO}_2)_4 \cdot \mathbf{L}_2$ that there are two peaks for absorption around 500~600 nm (band I) and 450 nm

(band II) in the visible region, which can be assigned to the allowed transitions, $\pi^* \rightarrow \sigma^*$ and $\pi^* \rightarrow \delta^*$, respectively⁷. Indeed, the band I was remarkably affected by the type of the axial ligands as shown in Figure 2-4-1, while the band II around 450 nm remained almost unchanged. The band II of $\mathbf{1} \cdot (\text{min})_2$ was overlapped by a large peak, which would be assigned to an MLCT between the dinuclear Rh-Rh center and the axial ligands. In comparison between the axial pyridine ligands with a substituent at the 2-position, $\mathbf{1} \cdot (\text{py})_2$, $\mathbf{1} \cdot (\text{mepy})_2$, and $\mathbf{1} \cdot (\text{etpy})_2$, bulkier axial ligands showed the absorption at a longer wavelength in the order of $\mathbf{1} \cdot (\text{py})_2$ (527 nm) < $\mathbf{1} \cdot (\text{mepy})_2$ (554 nm) < $\mathbf{1} \cdot (\text{etpy})_2$ (566 nm). On the other hand, only small electronic effects were observed with the axial pyridine ligands, $\mathbf{1} \cdot (\text{dmap})_2$ (red-shift by 7 nm) and $\mathbf{1} \cdot (\text{min})_2$ (blue-shift by 7 nm), which have an electron donating dimethylamino group and electron withdrawing methoxycarbonyl group, respectively, at the 4-position. It should be noted that the band I for $\mathbf{1} \cdot (\text{ether})_2$ appeared in the longest wavelength side (608 nm). This result indicates that the type of donor atoms of the axial ligands was one of the most effective factors affecting the absorption wavelength of the dinuclear Rh-Rh complexes. The steric repulsion would increase a distance between the axial ligands and the dinuclear core, and it would weaken the orbital interaction between them.

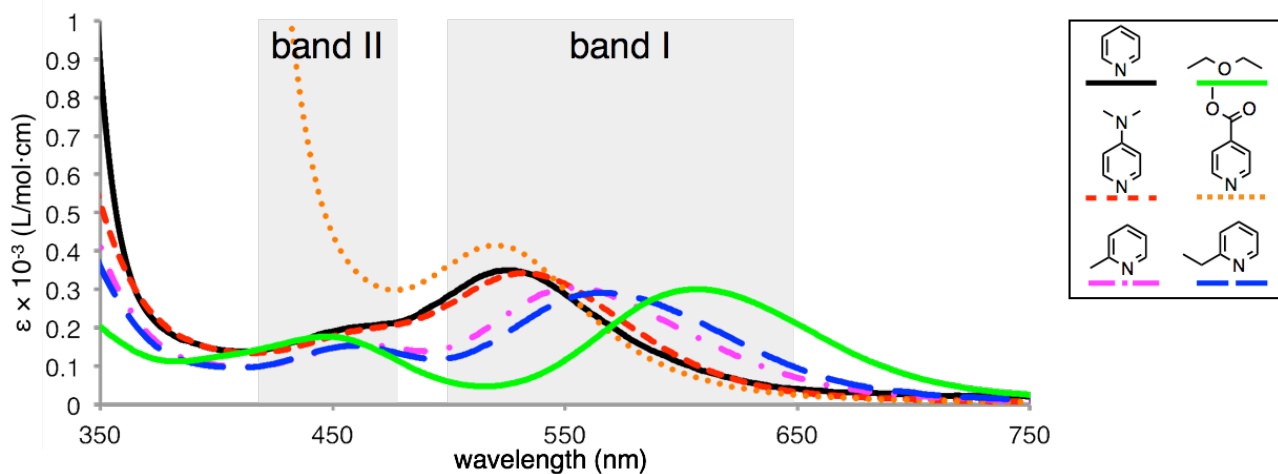


Figure 2-4-1. Visible absorption spectra of a molecular gear system $1 \cdot L_2$

2-5. NMR Study of a Gear System $1 \cdot L_2$

^1H NMR measurements of these obtained complexes were performed in CDCl_3 . Compared with carboxylic acid **2**, the signals of methyl groups at the 2,7,14-positions of triptycenes in each complex $1 \cdot L_2$ were shifted upfield (Figure 2-5-1). Observed upfield shifts of the signals in the ^1H NMR spectra are well explained by the shielding effect from the benzene rings of the adjacent triptycene parts, indicating a geared structure in the solution state.

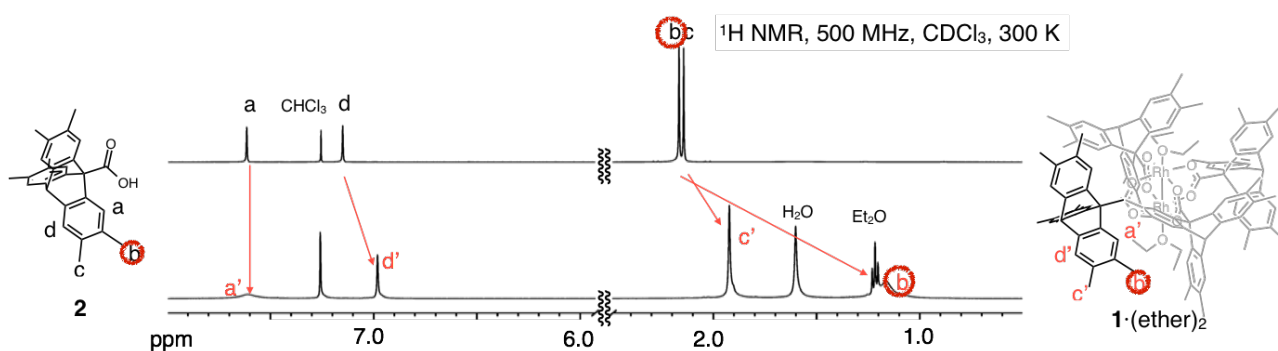


Figure 2-5-1. ^1H NMR spectra of a molecular gear system $1 \cdot (\text{ether})_2$ and carboxylic acid **2**

Then, the temperature effects on the rotational behaviors of the triptycene gear parts were examined by variable-temperature ^1H NMR (VT-NMR) spectroscopy. For instance, the ^1H NMR spectrum of 2-methylpyridine adduct $\mathbf{1}\cdot(\text{mepy})_2$ at 300 K showed broadened signals assigned to the protons a and b (Figure 2-5-2). When the temperature was lowered, all the signals eventually became broadened and then split. The spectrum at 260 K showed splitting of all the signals assigned to the blades of the triptycene parts. Similar splitting was observed in the spectra of a 2-ethylpyridine adduct $\mathbf{1}\cdot(\text{etpy})_2$ and $\mathbf{1}\cdot(\text{ether})_2$ (Figure 2-5-3 and Figure 2-5-4). The spectra of a pyridine adduct $\mathbf{1}\cdot(\text{py})_2$, an *N,N*-dimethyl-4-aminopyridine adduct $\mathbf{1}\cdot(\text{dmap})_2$ and a methyl isonicotinate adduct $\mathbf{1}\cdot(\text{min})_2$, however, showed no splitting at 220 K. This result suggests that the rotational behaviors were markedly affected by the type of axial ligands. VT-NMR measurements at low temperatures revealed the stable conformation of the triptycene parts may be a zigzag conformation because the signals of the blade split into a 2:1 (upfield/downfield) ratio (Figure 2-5-5). Although the other tongue-in-groove conformation also showed 2:1 splitting, in that case, the signals of a benzene ring of triptycene shielded by two benzene rings of the adjacent triptycene parts were expected to shift to upfield shift, and the ratio should become 1:2 (upfield/downfield).

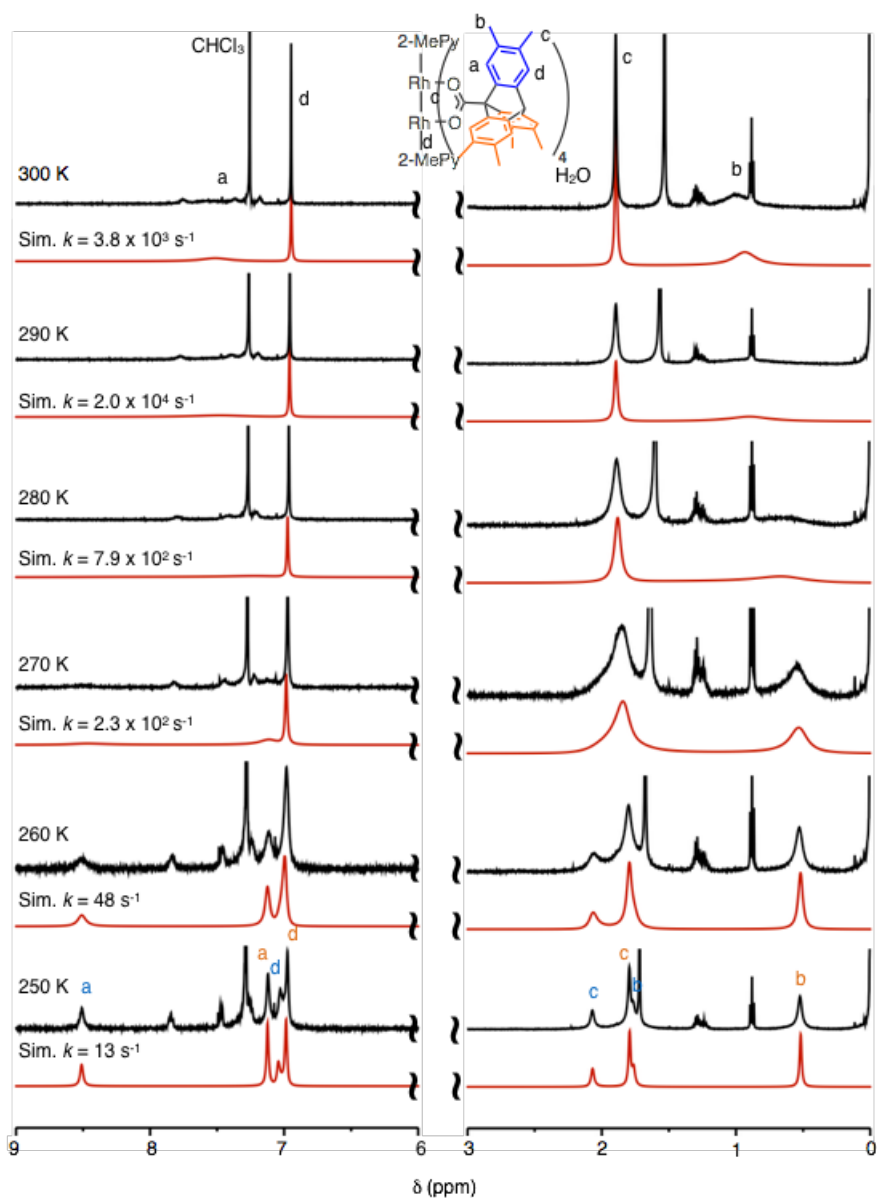


Figure 2-5-2. VT- ^1H NMR spectra of a molecular gear system $1 \cdot (\text{mepy})_2$ and dynamic ^1H NMR line shape simulations (Sim) using the iNMR software (version 5.3.3)

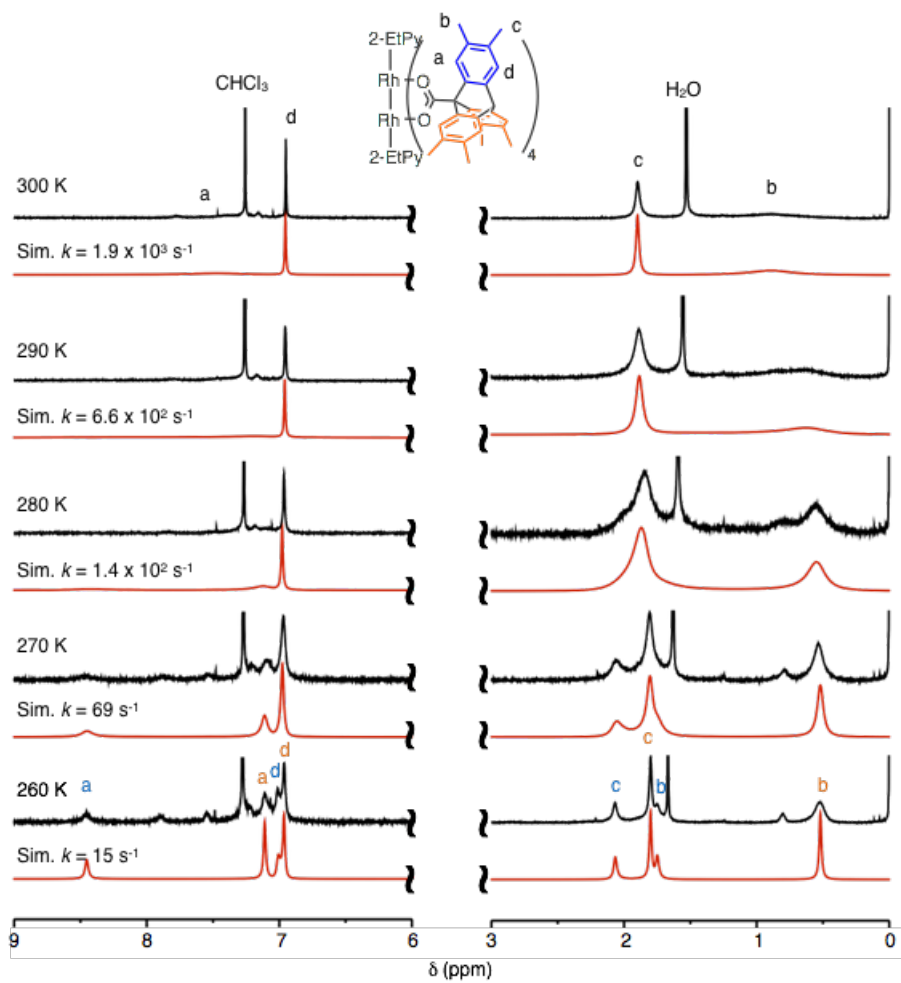


Figure 2-5-3. VT-¹H NMR spectra of a molecular gear system **1**·(etpy)₂ and dynamic ¹H NMR line shape simulations (Sim) using the iNMR software (version 5.3.3)

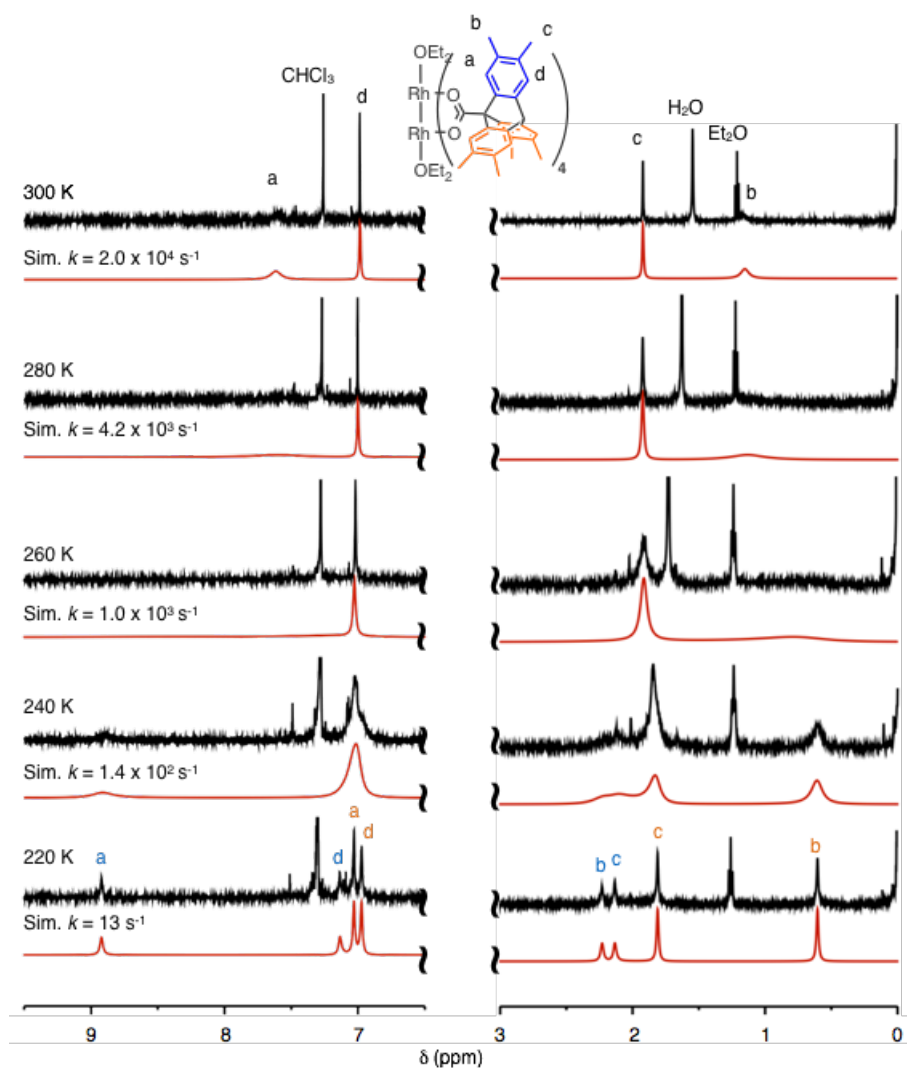


Figure 2-5-4. VT-¹H NMR spectra of a molecular gear system **1**·(ether)₂ and dynamic ¹H NMR line shape simulations (Sim) using the iNMR software (version 5.3.3)

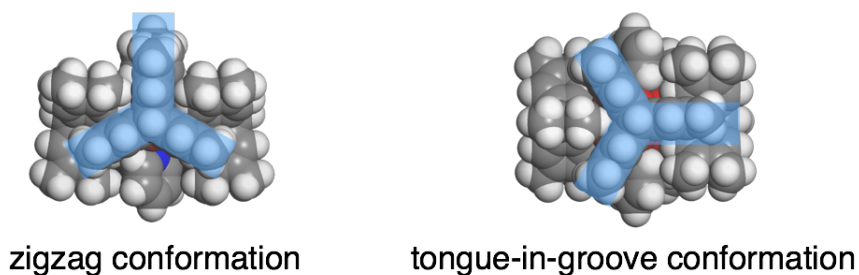


Figure 2-5-5. Illustrations of zigzag and tongue-in-groove conformations

The rotational rates of these complexes at a given temperature were determined by dynamic NMR experiments. Dynamic ^1H NMR line shape simulation was carried out based on the pairs of chemical shifts of splitting signals and the chemical exchange rates. When the chemical exchange rates are changed, the line shape of the simulated spectrum is changed. The 2:1 splitting signals assigned to equatorial and axial blades of triptycene parts were exchanged with each other by 60° rotation. The activation energy parameters were determined from the temperature dependence of the changes in the spectra of $\mathbf{1}\cdot(\text{mepy})_2$, $\mathbf{1}\cdot(\text{etpy})_2$, and $\mathbf{1}\cdot(\text{ether})_2$. The rotational rates and activation parameters for $\mathbf{1}\cdot(\text{py})_2$, $\mathbf{1}\cdot(\text{dmap})_2$, and $\mathbf{1}\cdot(\text{min})_2$ could not be determined because no splitting was observed in the NMR measurement at low temperatures due to their fast rotation compared with the NMR timescale. As for these three complexes, the activation energy barrier (ΔG^\ddagger) can be roughly estimated to be lower than 12 kcal mol^{-1} from the chemical shift gap $\Delta\nu > 0.1 \text{ ppm}$ and the coalescence temperature $T_c < 220 \text{ K}$ according to the following equation from the Eyring equation, where T_c is the coalescence temperature⁶.

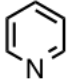
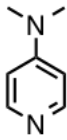
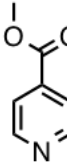
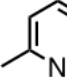
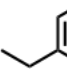
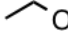
$$\Delta G^\ddagger = 4.55 \times 10^{-3} \times T_c \{9.97 + \log T_c - \log(500 \times \Delta\nu)\} [\text{kcal mol}^{-1}]$$

The rotational rates of the molecular gear complexes with pyridine derivatives were expected to vary with the steric effects of the substituents at the 2-positions of the pyridines (Table 2-5-6), which would enable steric control by the axial ligands. The activation enthalpies are increased with the steric repulsion because the steric repulsion increased the internal energies. The activation entropies seemed to have a similar tendency. They would depend on the conformation of the axial ligands in the transition state (Figure 2-5-7). In the ground state, the pyridine derivatives could have a conformation (asymmetrical pyridine derivatives can have two conformations) because of the walls of the axial blades of triptycene gears. In the transition state, the axial ligands could have

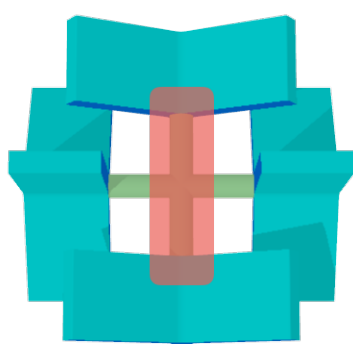
twice conformations due to the conformational change of the triptycene gears.

Moreover, further splitting was observed in the spectra of $1 \cdot (\text{mepy})_2$ and $1 \cdot (\text{etpy})_2$ at 220 K (Figure 2-4-8). This observation may come from the direction of unsymmetrical axial ligands in the slower rotation.

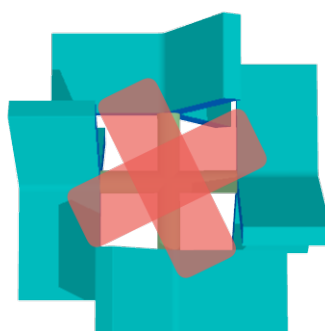
Table 2-5-6. Thermodynamic parameters of the gearing system $1 \cdot L_2$

L	 py	 dmap	 min	 mepy	 etpy	 ether
ΔH^\ddagger (kcal mol ⁻¹)	n.a.	n.a.	n.a.	14.5 ± 1.2	18.0 ± 0.5	11.4 ± 0.2
ΔS^\ddagger (cal mol ⁻¹ K ⁻¹)	n.a.	n.a.	n.a.	6 ± 4	16.6 ± 1.9	-0.8 ± 0.8
k_{rot} at 300 K (s ⁻¹)	n.a.	n.a.	n.a.	3.8 × 10 ³	1.9 × 10 ³	2.0 × 10 ⁴

n.a. = not available



zigzag conformation
= ground state



tongue-in-groove conformation
= transition state

Figure 2-5-7 Conformation of the axial ligands in ground and transition states

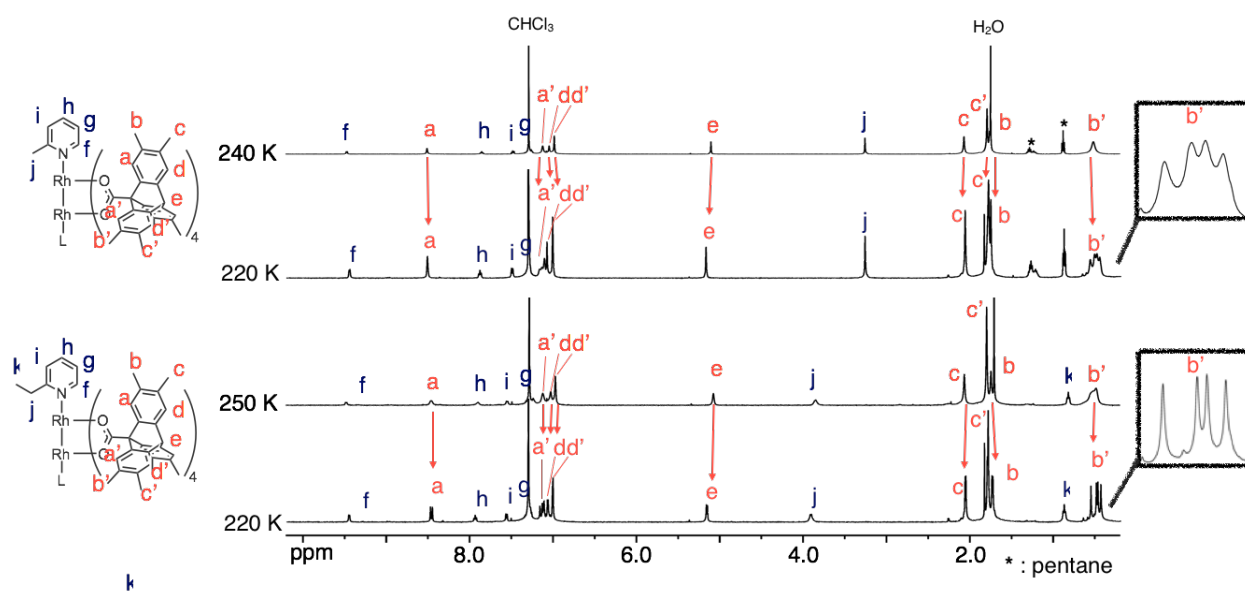


Figure 2-5-8 Further splitting in ^1H NMR spectra of molecular gear systems $1 \cdot (\text{mepy})_2$ and $1 \cdot (\text{etpy})_2$

2-6. References

1. J. N. van Niekerk, F. R. L. Schoening, *Acta Cryst.* **1953**, *6*, 227–232.
2. E. B. Boyar, S. D. Robinson, *Coord. Chem. Rev.* **1983**, *50*, 109–208.
3. S. Friedle, J. J. Kodanko, K. L. Fornace, S. J. Lippard, *J. Mol. Struct.* **2008**, *890*, 317–327.
4. S. Vagin, A. Ott, H.-C. Weiss, A. Karbach, D. Volkmer, B. Rieger, *Eur. J. Inorg. Chem.* **2008**, 2601–2609.
5. A. Demonceau, A. F. Noels, A. J. Hubert, P. Teyssié, *Bull. Soc. Chim. Belg.* **1994**, *93*, 945–948.
6. M. Hesse, H. Maier, B. Zeeh, *Spectroscopic Method in Organic Chemistry*; Thieme Publishing Group: Stuttgart, 2007.

7. Y. Kataoka, Y. Kitagawa, T. Saito, Y. Nakanishi, K. Sato, Y. Miyazaki, T. Kawakami, M. Okumura, W. Mori, K. Yamaguchi, *Supramol. Chem.* **2011**, *23*, 329–336.

2-7. Experimental Section

General Procedure

Unless otherwise noted, solvents and reagents were purchased from TCI Co., Ltd., WAKO Pure Chemical Industries Ltd., Kanto Chemical Co., Sigma-Aldrich Co., and Kojima Chemicals Co., Ltd., and used without further purification if not mentioned.

^1H , ^{13}C NMR, and other 2D NMR spectra were recorded on a Bruker AVANCE III-500 (500 MHz for ^1H) spectrometer. The following pulse programs were used with default parameters: zg30 (^1H), zgpg30 (^{13}C). Tetramethylsilane was used as an internal standard (δ 0 ppm) for ^1H and ^{13}C NMR measurements when CDCl_3 was used as a solvent. A residual solvent signal was used for calibration of ^1H and ^{13}C NMR measurements when $\text{DMSO}-d_6$ (δ 2.50 ppm for ^1H NMR and 39.7 ppm for ^{13}C NMR) was used as a solvent^{S1}.

Single crystals in paratone-N oil were mounted on a nylon loop. Single crystal X-ray crystallographic analyses were performed using a Rigaku RAXIS-RAPID imaging plate diffractometer with $\text{MoK}\alpha$ radiation ($\lambda = 0.71073 \text{ \AA}$), and obtained data were calculated using the Crystal Structure crystallographic software package except for refinement, which was performed using SHELXL-97 and SHELXL-2013^{S2}. Strains (bond distances, angles, and displacement parameters) were applied for disordered solvents. Main backbones were refined anisotropically. All hydrogen atoms were replaced geometrically and refined using a riding model. Crystallographic

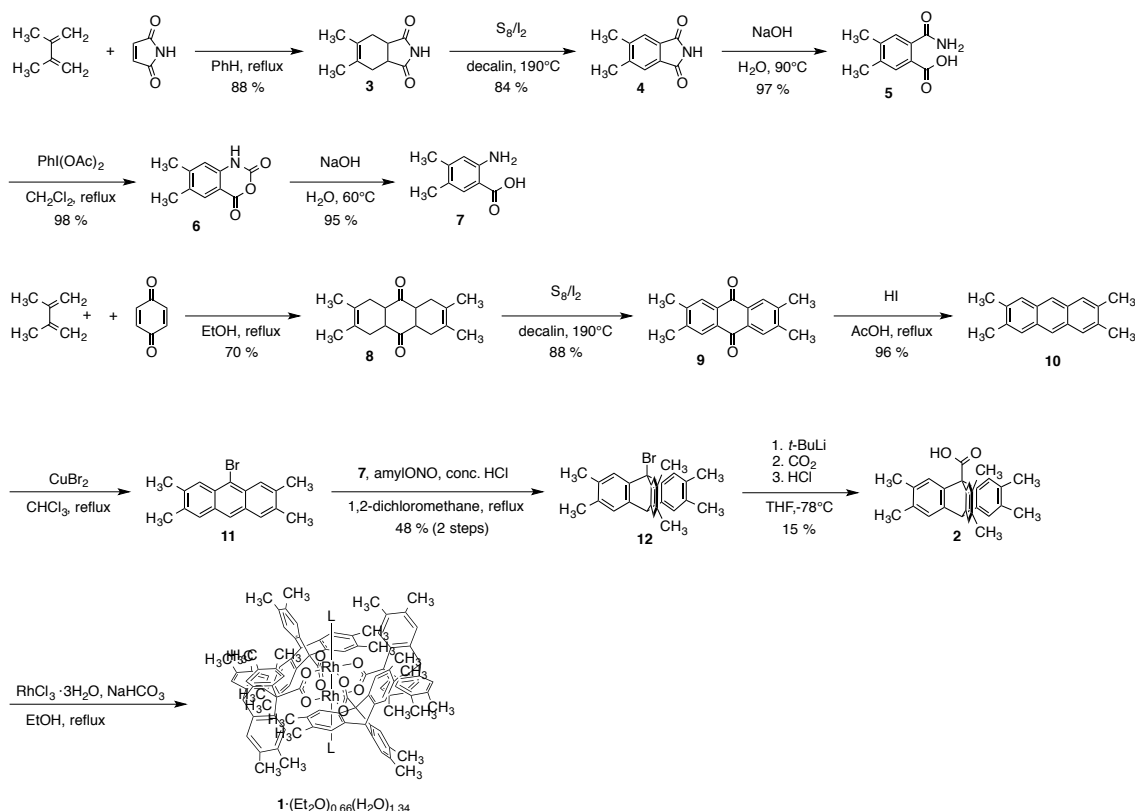
data in this paper can be obtained free of charge from the Cambridge Crystallographic Data Centre (http://www.ccdc.cam.ac.uk/data_request/cif).

ESI-TOF mass data were recorded on a Waters Micromass LCT Premier XE mass spectrometer. Unless otherwise noted, experimental conditions were as follows (Ion mode, positive; Capillary voltage, 300 V; Sample cone voltage, 30 V; Desolvation temperature, 150 °C; Source temperature, 80 °C).

UV-Vis spectra were recorded on a HITACHI U-3500 UV-Vis spectrophotometer.

Synthesis of Molecular Gear System **1·L₂**

The molecular gear system **1**·L₂ was synthesized according to the Scheme 2-7-1. 4,5-Dimethylantranilic acid **7**^{S3-S5} and 9-bromo-2,3,6,7-tetramethylantracene **11**^{S2,S6-S8} were synthesized according to the literature procedure with slight modifications.



Scheme 2-7-1. Synthesis of a molecular gear system $1 \cdot L_2$

Synthesis of 4,5-Dimethyl- Δ -tetrahydrophthalimide (**3**)^{S3}

In a pressure bottle, a mixture of maleimide (4.03 g, 42 mmol) and 2,3-dimethyl-1,3-butadiene (10.4 mL, 92 mmol) in dry benzene (80 mL) was heated at reflux for 14 h, and then cooled to room temperature. The resulting mixture was evaporated and dried in vacuo to yield imide **3** as a white solid (6.57 g, 88%). This crude material was used for the next reaction without further purification.

^1H NMR (500 MHz; CDCl_3 ; 300 K): δ 7.80 (s, 1H), 3.09 (s, 2H), 2.43 (d, $J = 14.9$ Hz, 2H), 2.23 (d, $J = 13.9$ Hz, 2H), 1.69 (s, 6H); ^{13}C NMR (126 MHz; CDCl_3 ; 300 K): δ 180.1, 127.1, 41.3, 30.6, 19.5.

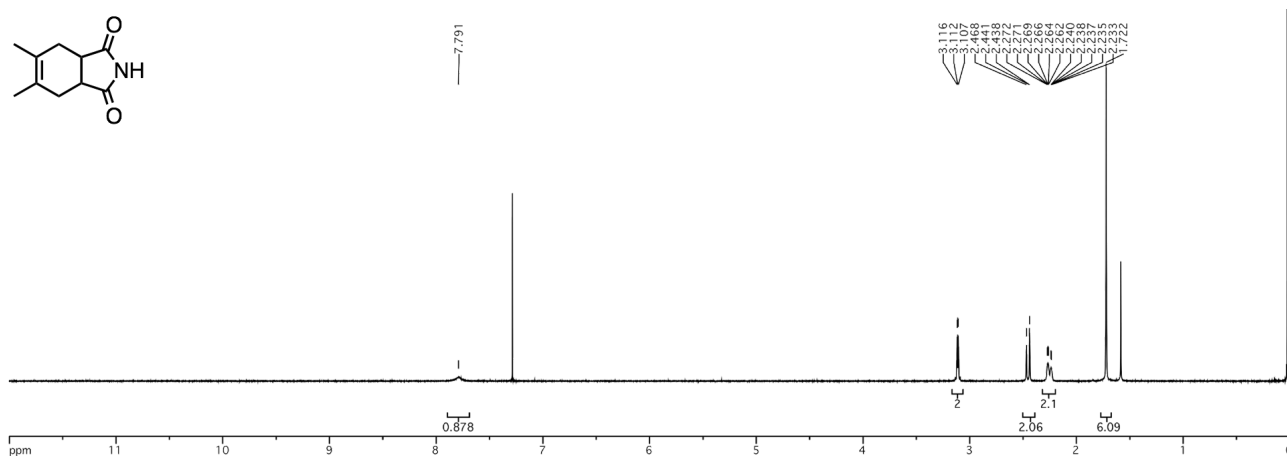


Figure 2-7-2. ¹H NMR spectrum of **3** (CDCl₃, 500 MHz, 300 K)

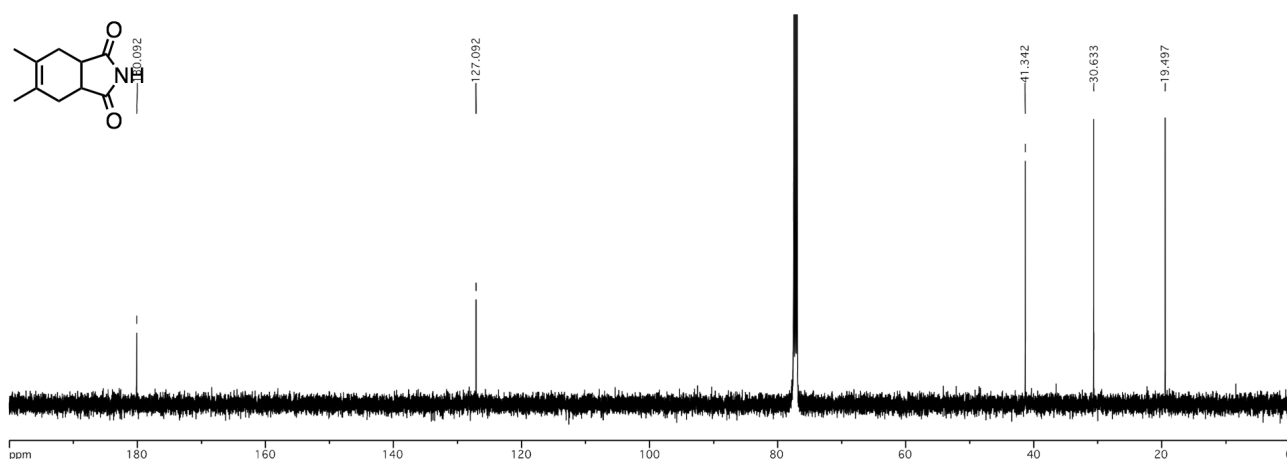


Figure 2-7-3. ¹³C NMR spectrum of **3** (CDCl₃, 126 MHz, 300 K)

Synthesis of 4,5-Dimethylphthalimide (**4**)^{S3}

To a stirred suspension of imide **3** (6.54 g, 37 mmol) and sulfur (2.90 g, 90 mmol) in diphenyl ether (1.5 mL) and decalin (39 mL) was added iodine (42 mg, 0.17 mmol), and then the mixture was heated at 190 °C for 15 h. The mixture was cooled to room temperature, filtered, washed with ether, and dried in vacuo to yield **4** as an orange solid (5.36 g, 84%). This material was used for the next reaction without further purification.

^1H NMR (500 MHz; CDCl_3 ; 300 K): δ 7.61 (s, 2H), 7.37 (s, 1H), 2.41 (s, 6H); ^{13}C NMR (126 MHz; CDCl_3 ; 300 K): δ 168.4, 144.3, 130.8, 124.7, 20.8.

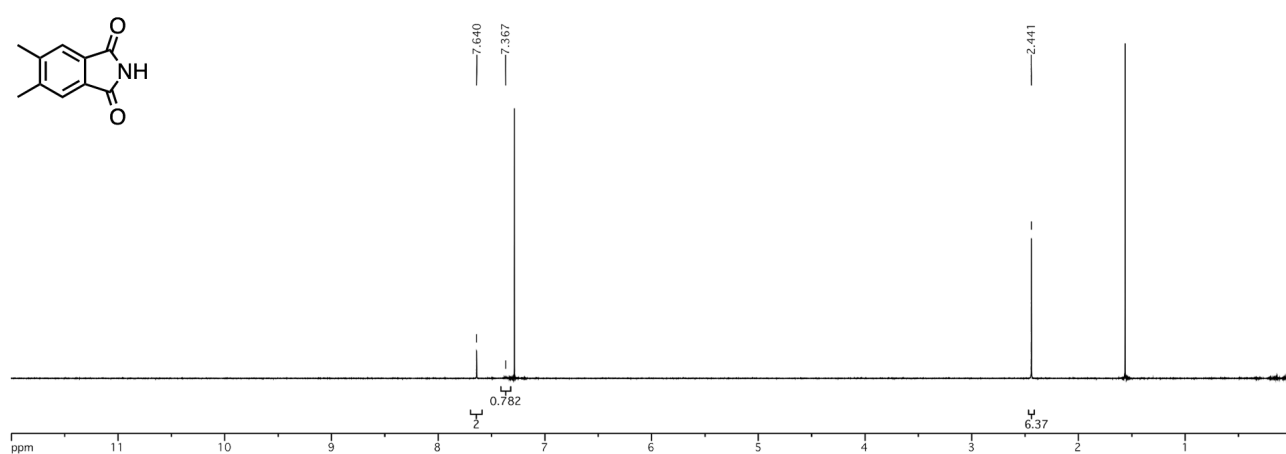


Figure 2-7-4. ^1H NMR spectrum of **4** (CDCl_3 , 500 MHz, 300 K)

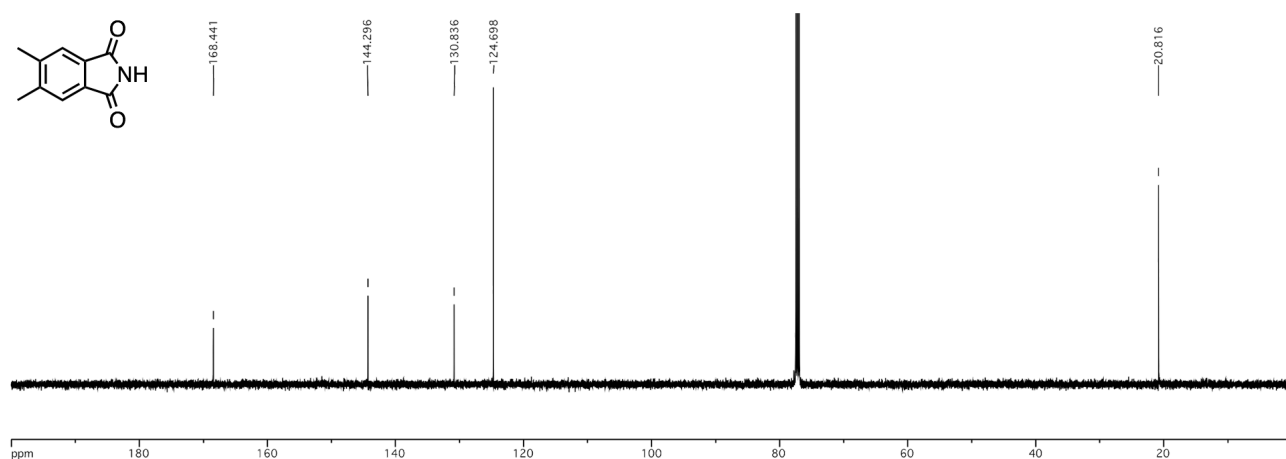


Figure 2-7-5. ^{13}C NMR spectrum of **4** (CDCl_3 , 126 MHz, 300 K)

Synthesis of 2-Carbamyl-4,5-dimethylbenzoic Acid (**5**)^{S3}

A mixture of phthalimide **4** (4.94 g, 27.5 mmol) in 1.0 M aqueous NaOH (30 mL, 30 mmol) was heated at 90 °C for 1 h. The solution was filtered while hot, cooled to room temperature, and then acidified by conc. HCl. The precipitate was collected and dried in vacuo to yield **5** as an

orange solid (5.16 g, 97%). This material was used for the next reaction without further purification.

^1H NMR (500 MHz; $\text{DMSO-}d_6$; 300 K): δ 12.68 (s, 1H), 7.67 (s, 1H), 7.49 (s, 1H), 7.23 (s, 2H), 2.27 (s, 3H), 2.26 (s, 3H); ^{13}C NMR (126 MHz; $\text{DMSO-}d_6$; 300 K): δ 170.3, 168.2, 139.5, 137.3, 136.0, 130.0, 128.5, 128.3, 19.2, 19.0.

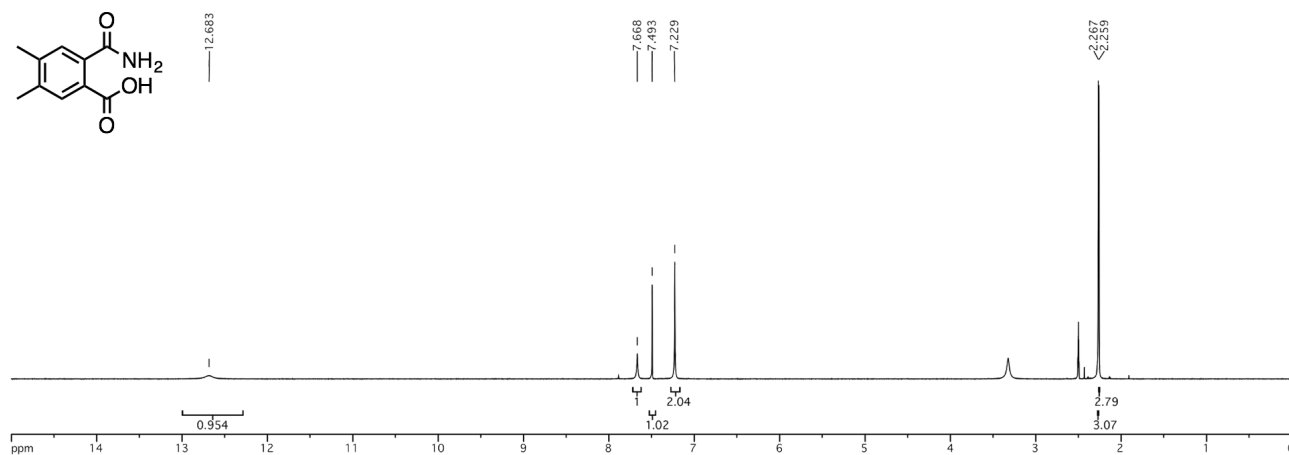


Figure 2-7-6. ^1H NMR spectrum of **5** ($\text{DMSO-}d_6$, 500 MHz, 300 K)

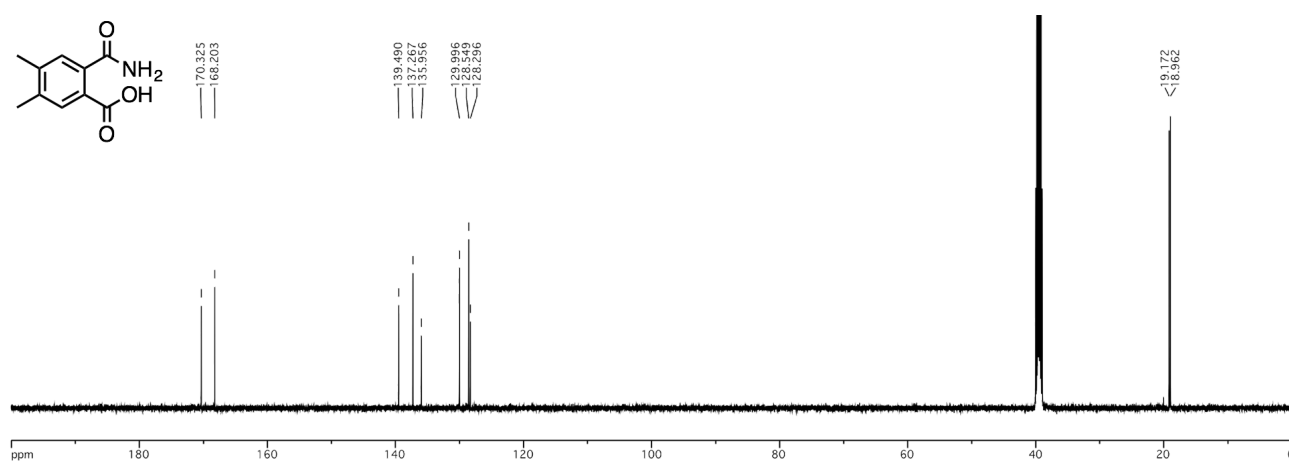


Figure 2-7-7. ^{13}C NMR spectrum of **5** ($\text{DMSO-}d_6$, 126 MHz, 300 K)

Synthesis of 6,7-Dimethyl-1*H*-benzo[*d*][1,3]oxazine-2,4-dione (**6**)^{S4}

To a stirred mixture of **5** (17.1 g, 88.5 mmol) in CH_2Cl_2 (250 mL) was added iodobenzene

diacetate (32.2 g, 100 mmol). The mixture was heated at reflux for 5 h, and then cooled to room temperature. After filtration and washing with CH_2Cl_2 until the liquid phase became colorless, the solvents were removed and dried in vacuo to yield dione **6** as an off-white solid (16.5 g, 98%). This material was used for the next reaction without further purification.

^1H NMR (500 MHz; $\text{DMSO-}d_6$; 300 K): δ 10.50 (s, 1H), 7.67 (s, 1H), 6.92 (s, 1H), 2.29 (s, 3H), 2.24 (s, 3H); ^{13}C NMR (126 MHz; $\text{DMSO-}d_6$; 300 K): δ 160.2, 147.84, 147.78, 140.0, 132.8, 129.1, 116.1, 108.1, 20.6, 19.0.

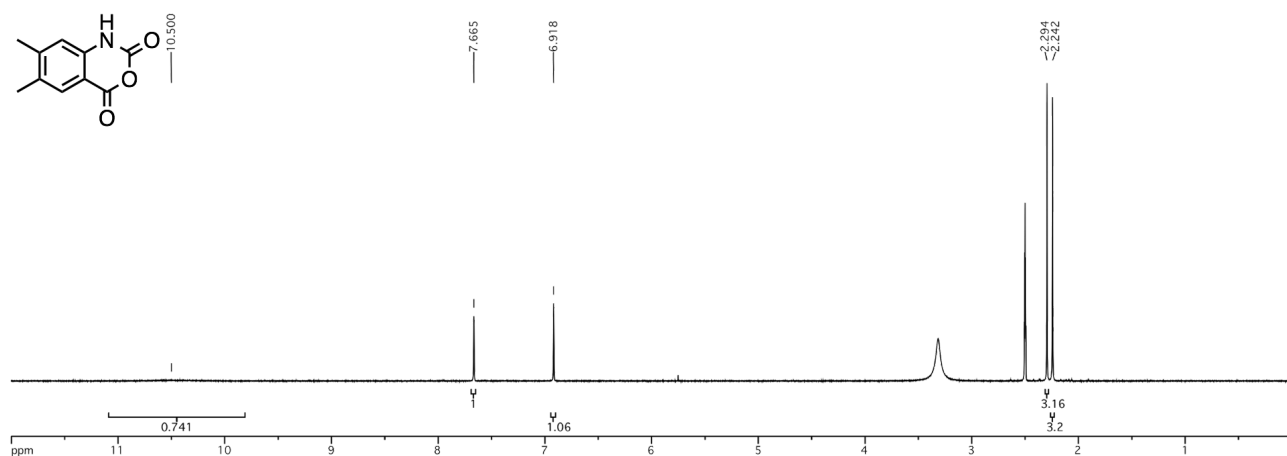


Figure 2-7-8. ^1H NMR spectrum of **6** ($\text{DMSO-}d_6$, 500 MHz, 300 K)

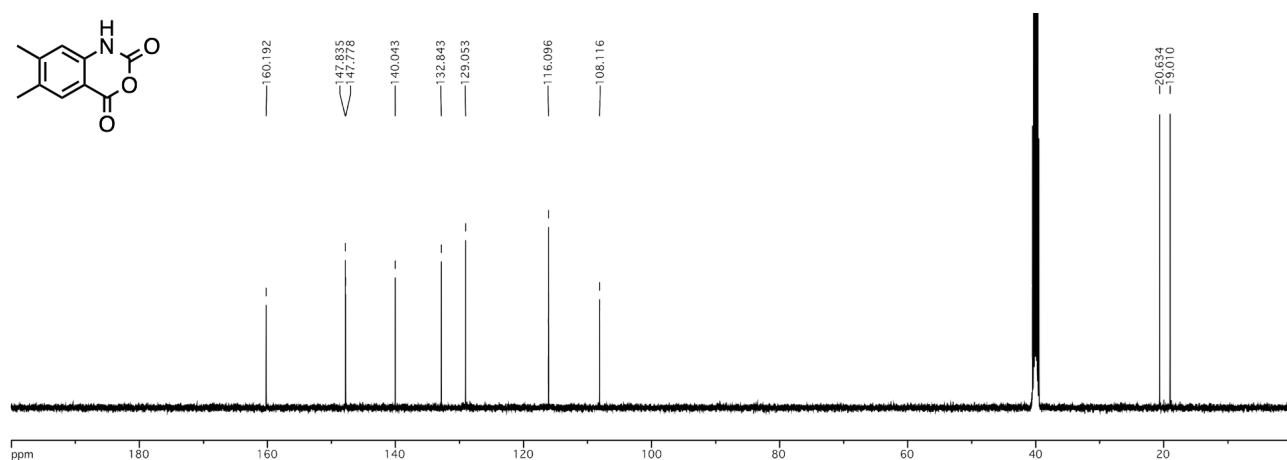


Figure 2-7-9. ^{13}C NMR spectrum of **6** ($\text{DMSO-}d_6$, 126 MHz, 300 K)

Synthesis of 4,5-Dimethylantranilic Acid (**7**)^{S3}

A mixture of dione **6** (2.37 g, 12.4 mmol) in 0.5 M aqueous NaOH (100 mL, 50 mmol) was heated at 60 °C. After 2 h, the mixture was heated at reflux for 30 min. After cooling to room temperature, the mixture was acidified to pH 4 by acetic acid. The precipitate was collected, washed by water, and dried in vacuo to yield anthranilic acid **7** as an orange solid (1.94 g, 95%). This material was used for the next reaction without further purification.

¹H NMR (500 MHz; DMSO-*d*₆; 300 K): δ 8.31 (s, 2H), 7.43 (s, 1H), 6.52 (s, 1H), 2.11 (s, 3H), 2.06 (s, 3H); ¹³C NMR (126 MHz; DMSO-*d*₆; 300 K): δ 169.7, 149.9, 143.1, 131.3, 122.5, 117.3, 107.6, 19.9, 18.4; LRMS (CH₃CN, negative, capillary: 3000 V, sample cone: 30 V): [**7**·H]⁺ (C₂₇H₂₅O₂) *m/z* 166.1 (required, 166.1).

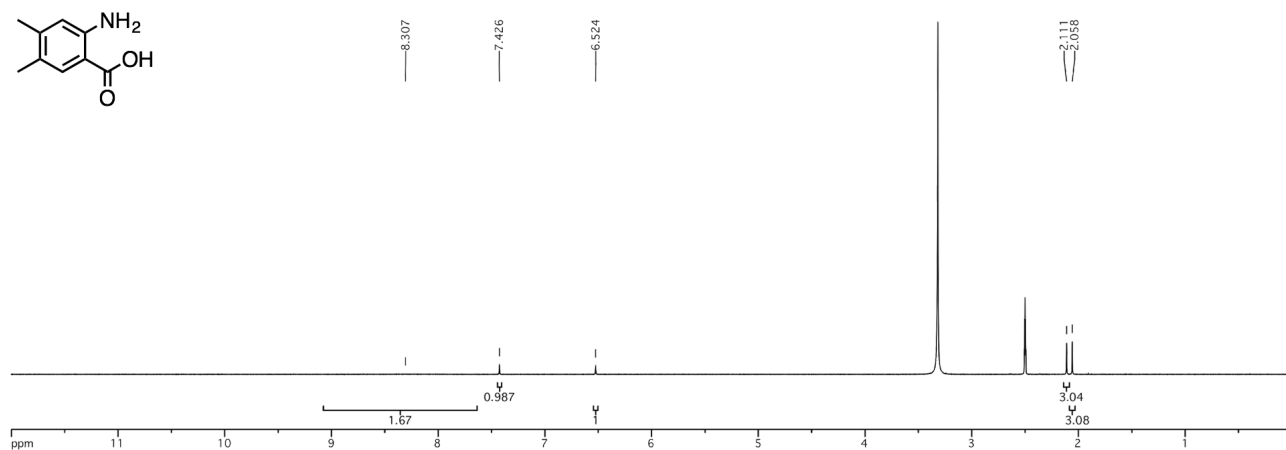


Figure 2-7-10. ¹H NMR spectrum of **7** (DMSO-*d*₆, 500 MHz, 300 K)

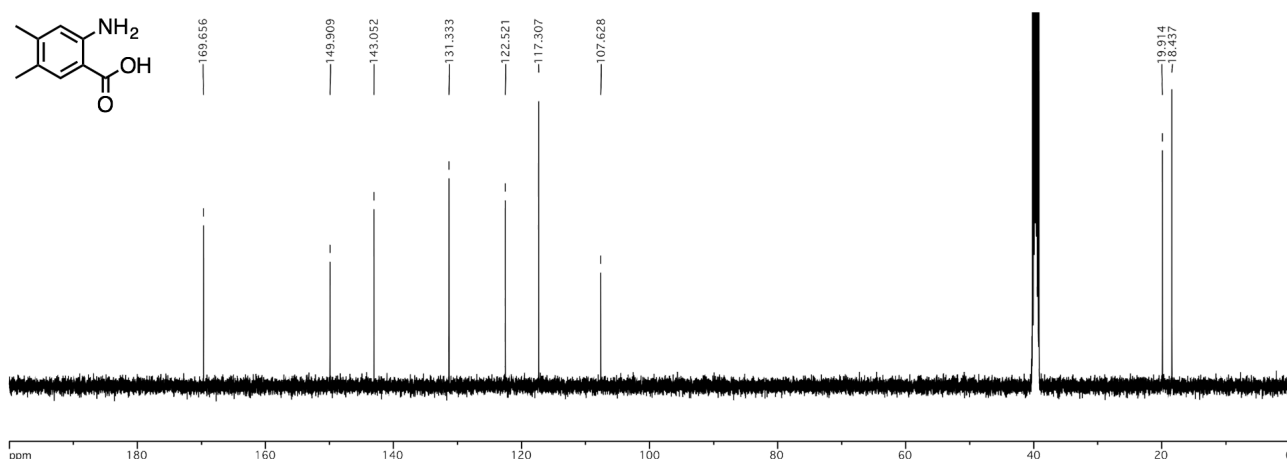


Figure 2-7-11. ¹³C NMR spectrum of 7 (DMSO-*d*₆, 126 MHz, 300 K)

Synthesis of 1,4,5,8,9a,10a-Octahydro-2,3,6,7-tetramethyl-9,10-anthraquinone (8)^{S6}

In a pressure tube, a mixture of 2,3-dimethyl-1,3-butadiene (0.90 g, 8.0 mmol) and 1,4-benzoquinone (217 mg, 2.0 mmol) in ethanol (4 mL) was heated at reflux for 19 h. The mixture was cooled with a cold bath, filtered, washed with ethanol, and dried in vacuo to yield hydroanthraquinone **8** as a white solid (381 mg, 70%). This material was used for the next reaction without further purification.

¹H NMR (500 MHz; CDCl₃; 300 K): δ 3.00-2.95 (m, 4H), 2.38 (dd, *J* = 16.0, 3.4 Hz, 4H), 2.10 (dd, *J* = 15.7, 3.7 Hz, 4H), 1.61 (s, 12H); ¹³C NMR (126 MHz; CDCl₃; 300 K): δ 210.9, 123.5, 44.8, 30.3, 19.0.

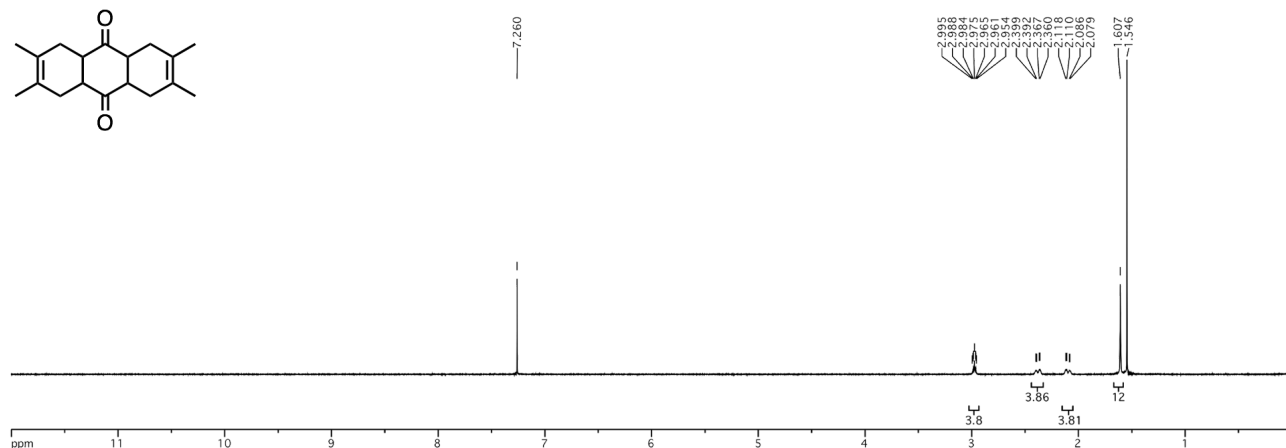


Figure 2-7-12. ^1H NMR spectrum of **8** (CDCl_3 , 500 MHz, 300 K)

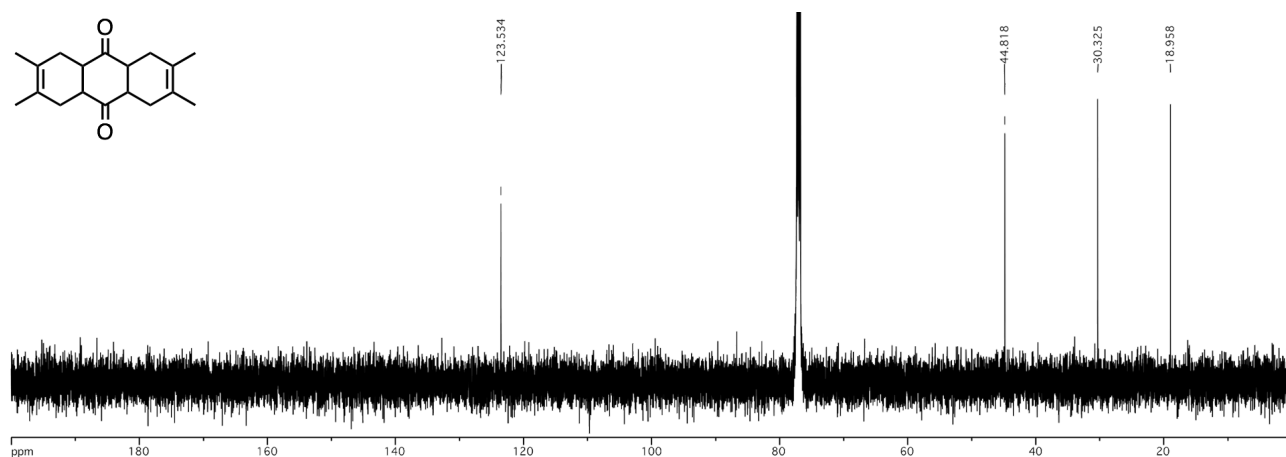


Figure 2-7-13. ^{13}C NMR spectrum of **8** (CDCl_3 , 126 MHz, 300 K)

Synthesis of 2,3,6,7-Tetramethyl-9,10-anthraquinone (**9**)^{S6}

To a stirred suspension of hydroanthraquinone **8** (3.05 g, 11.2 mmol) and sulfur (1.61 g, 6.29 mmol) in diphenyl ether (0.8 mL) and decalin (25 mL) was added iodine (41 mg, 0.16 mmol), and then the mixture was heated at 190 °C. When the mixture formed a solid, additional decalin (26 mL) was added. After refluxing for 5.5 h, the mixture was cooled to room temperature, filtered, washed with ether, and dried in vacuo to yield a greenish solid. The solid was ground and added to

the filtrate. To the mixture was added iodine (46 mg, 0.18 mmol), and then the mixture was heated at 190 °C for 12 h, cooled to room temperature, filtered, washed with ether, and dried in vacuo to yield a black solid. The solid was purified by short-path column chromatography (CH₂Cl₂ as eluent) to yield anthraquinone **9** as a greenish solid (2.60 g, 88%). This material was used for the next reaction without further purification.

¹H NMR (500 MHz; CDCl₃; 300 K): δ 8.03 (s, 4H), 2.43 (s, 12H); ¹³C NMR (126 MHz; CDCl₃; 300 K): δ 183.6, 143.7, 131.7, 128.1, 20.2.

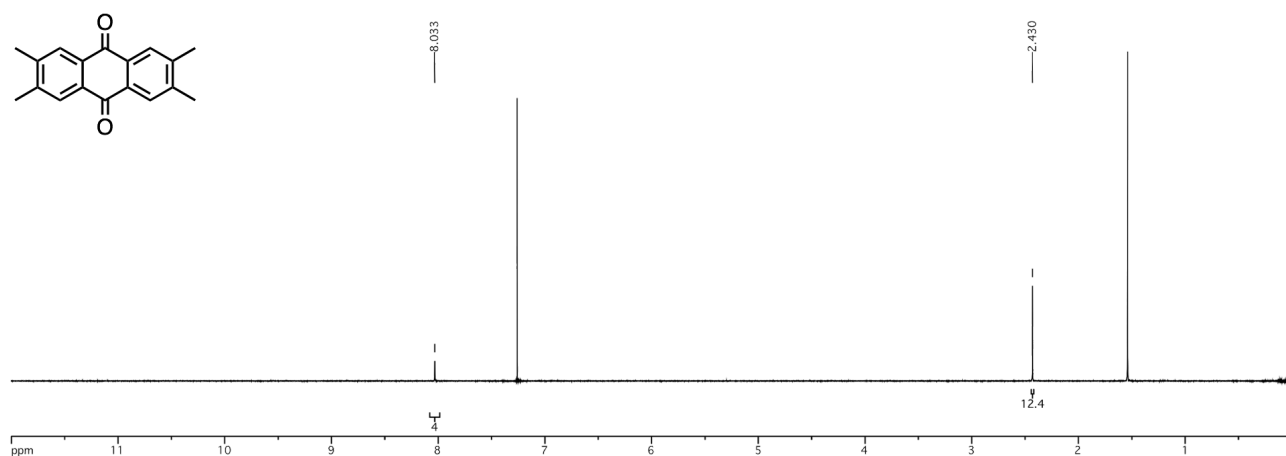


Figure 2-7-14. ¹H NMR spectrum of **9** (CDCl₃, 500 MHz, 300 K)

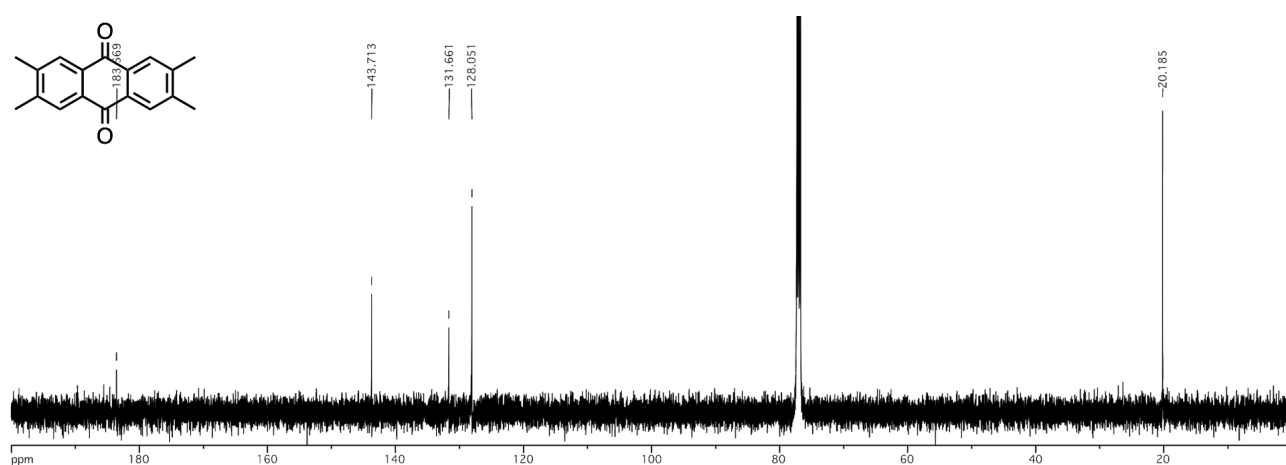


Figure 2-7-15. ¹³C NMR spectrum of **9** (CDCl₃, 126 MHz, 300 K)

Synthesis of 2,3,6,7-Tetramethylantracene (**10**)^{S6}

A degassed mixture of anthraquinone **9** (1.53 g, 5.78 mmol) in 55% hydroiodic acid (15 mL) and acetic acid (50 mL) was shielded and heated at reflux for 3 days under argon. After cooling to room temperature, the mixture was poured into saturated Na₂SO₃ solution (200 mL). The solid precipitated was collected by a filter, washed with water, and dried in vacuo to yield anthracene **10** as a greenish solid (1.31 g, 96%). This material was used for the next reaction without further purification.

¹H NMR (500 MHz; CDCl₃; 300 K): δ 8.15 (s, 2H), 7.70 (s, 4H), 2.45 (s, 12H); ¹³C NMR was not detected due to the low solubility in chloroform-*d*₁.

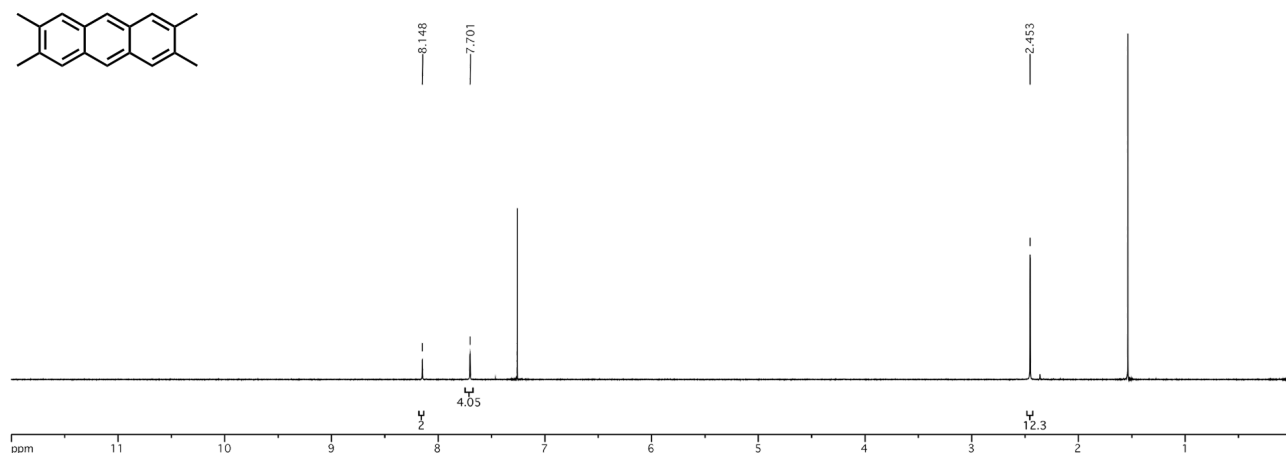
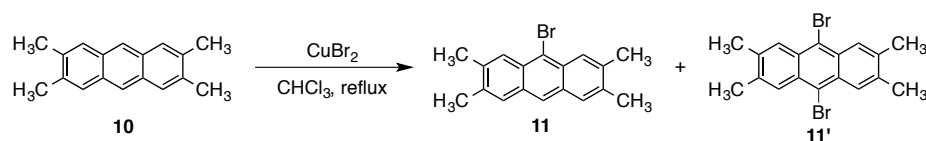


Figure 2-7-16. ¹H NMR spectrum of **10** (CDCl₃, 500 MHz, 300 K)

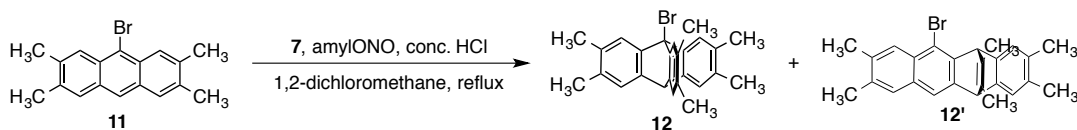
Synthesis of 2,3,6,7,14,15-Hexamethyltritycene-9-carboxylic Acid (**2**)



To a stirred mixture of anthracene **10** (235 mg, 1.00 mmol) in dry CHCl₃ (10 mL) was added

CuBr₂ (461 mg, 2.06 mmol) under argon. The mixture was heated at 50 °C for 15 h under argon, and then cooled to room temperature. The solution was filtered through a pad of celite, and the residue was washed with CH₂Cl₂ until the washing became colorless. The filtrate was dried over Na₂SO₄, evaporated, and dried in vacuo to yield a yellow-green solid (284 mg). The crude was purified by flash column chromatography (φ40 x 75 mm, *n*-hexane as eluent) to afford a 2:9:1 mixture of **10**/**11**/**11'** as a yellow solid (which would contain about 175 mg of **11** (56%)). The ratio was determined by ¹H NMR spectrum. The mixture was used in the next step without further purification.

¹H NMR of **11** (500 MHz; CDCl₃; 300 K): δ 8.20 (s, 2H), 8.16 (s, 1H), 7.69 (s, 2H), 2.51 (s, 6H), 2.47 (s, 6H).

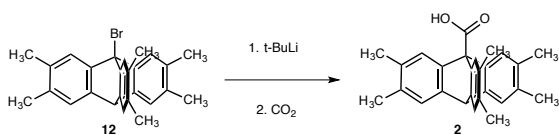


To a stirred mixture of acid **7** (634 mg, 3.9 mmol) and conc. HCl (0.4 mL) and ethanol (9.4 mL) with ice bath cooling was added dropwise isoamyl nitrite (1.0 mL, 7.5 mmol). After 3 h, the suspension of diazonium carboxylate was decanted with Et₂O, and then replaced by dry 1,2-dichloroethane.

To a refluxed solution of anthracene derivatives, obtained in the previous step (236 mg containing 0.51 mmol of **11**, 0.12 mmol of **10**, and 0.12 mmol of **11'**), and chloromethyloxirane (0.5 mL, 6.4 mmol) in dry 1,2-dichloroethane (10 mL) was added the betain suspension. After addition of approximately 4 equiv. of the diazonium carboxylate, TLC indicated the disappearance of anthracenes. The solution was cooled to room temperature, and washed with saturated aq. NaHCO₃ (20 mL) and water, and dried over Na₂SO₄. After evaporation, the crude material was

separated by flash column chromatography ($\phi 55 \times 75$ mm, 100:1 *n*-hexane/ CH_2Cl_2 as eluent) to afford a mixture of triptycene **12** and byproduct **12'** (ca. 93:7 judged by ^1H NMR) as a white solid (184 mg). This mixture was used in the next step without further purification.

^1H NMR of **12** (500 MHz; CDCl_3 ; 300 K): δ 7.49 (s, 3H), 7.11 (s, 3H), 5.18 (s, 1H), 2.16 (s, 9H), 2.14 (s, 9H); ^{13}C NMR of **12** (126 MHz; CDCl_3 ; 300 K): δ 142.4, 141.6, 133.9, 132.9, 124.9, 124.2, 70.9, 52.2, 19.5, 19.2.



To a stirred mixture of 1.5 M solution of *t*-BuLi in pentane (0.08 mL, 0.12 mmol) and dry THF (2 mL) was added dropwise a solution of bromotriptycene **12** (21 mg, 0.05 mmol) in dry THF (2 mL) at -78 °C under argon. After 15 min, CO_2 gas passed through CaCl_2 was introduced into the reaction container for 5 min, and then the mixture was allowed to warm to room temperature. The reaction was quenched with 1.0 M HCl, extracted with CH_2Cl_2 (5 mL \times 3), dried over Na_2SO_4 , evaporated, and dried in vacuo to yield a yellow solid (19 mg). The crude material was purified by flash column chromatography ($\phi 5 \times 30$ mm, 100:1 $\text{CH}_2\text{Cl}_2/\text{MeOH}$ as eluent). The obtained pale yellow solid was washed by 5:1 *n*-hexane/ CH_2Cl_2 to afford **2** as a white solid (2.8 mg, 7% from **10**).

^1H NMR (500 MHz; CDCl_3 ; 300 K): δ 7.49 (s, 3H), 7.11 (s, 3H), 5.18 (s, 1H), 2.16 (s, 9H), 2.14 (s, 9H); ^{13}C NMR (126 MHz; CDCl_3 ; 300 K): δ 142.4, 141.6, 133.9, 132.9, 124.9, 124.2, 70.9, 52.2, 19.5, 19.2; LRMS (CH_3CN , negative, capillary: 3000 V, sample cone: 30 V): 2^- ($\text{C}_{27}\text{H}_{25}\text{O}_2$) m/z 381.2 (required, 381.2).

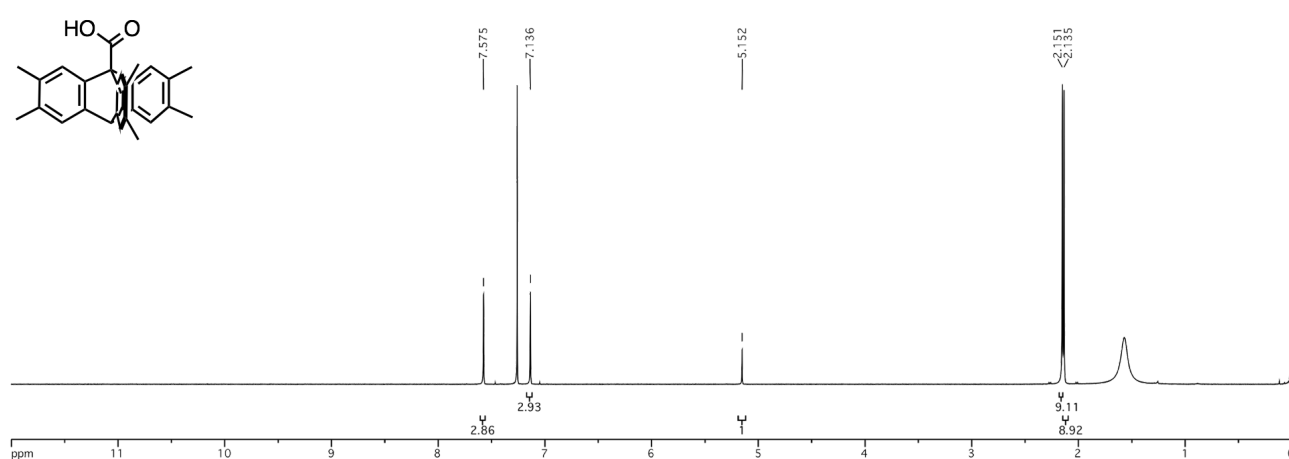


Figure 2-7-17. ^1H NMR spectrum of **2** (CDCl₃, 500 MHz, 300 K)

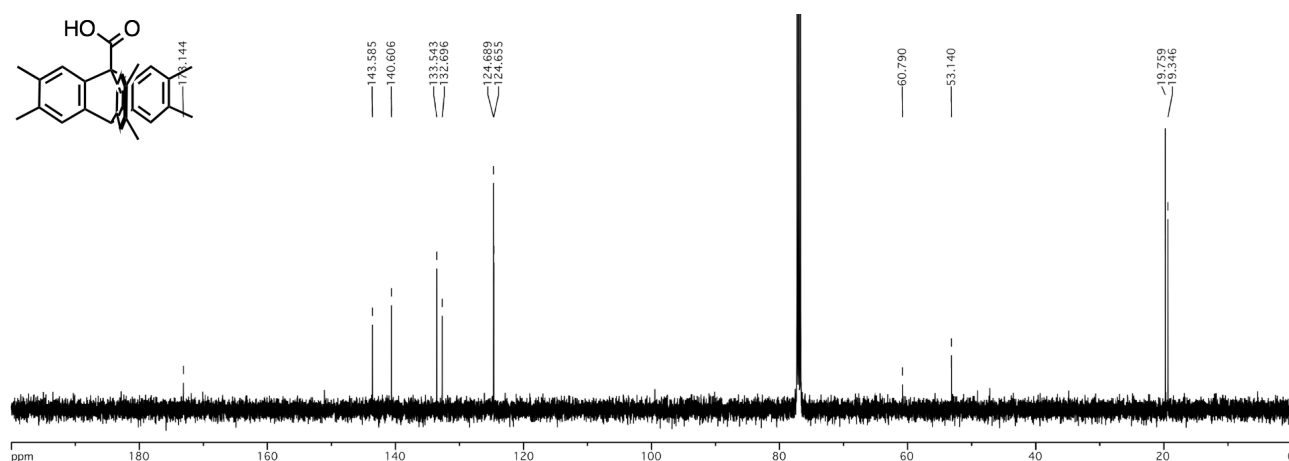


Figure 2-7-18. ^{13}C NMR spectrum of **2** (CDCl₃, 126 MHz, 300 K)

Synthesis of Molecular Gearing System 1

Diethyl ether adduct **1**·(ether)₂

A mixture of rhodium(III) chloride trihydrate (227 mg, 0.86 mmol), sodium hydrogen carbonate (182 mg, 2.16 mmol) and carboxylic acid **2** (828 mg, 2.16 mmol) in ethanol (20 mL) was heated at reflux for 24 h. Then, the solvent was evaporated and the crude was purified by column chromatography (ϕ 30 x 90 mm, 10:1 *n*-hexane/AcOEt as eluent) to give a green solid. The solid

was recrystallized from Et₂O/CH₂Cl₂ and dried in vacuo at 150 °C to yield **1**·(Et₂O)_{0.64}(H₂O)_{1.34} as a green solid (376 mg, 48%).

¹H NMR (500 MHz; CDCl₃; 300 K): δ 7.78-7.40 (br, 12H), 6.98 (s, 12H), 5.02 (s, 4H), 3.48 (q, *J* = 7.0 Hz, 3H), 1.92 (s, 36H), 1.32-1.01 (m, 41H); elemental analysis of **1**·(Et₂O)_{0.64}(H₂O)_{1.34}: Calcd for C_{110.64}H_{109.24}O₁₀Rh₂: C, 73.63; H, 6.10; N, 0.00. Found: C, 73.71; H, 6.42; N, 0.00; LRMS (CHCl₃ + NaI in IPA, negative, capillary: 1000 V, sample cone: 10 V): [**1**·I]⁻ (C₁₀₈H₁₀₀O₈Rh₂I) *m/z* 1858.4 (required, 1858.5).

*Only monoiodite adduct [**1**·I]⁻ was detected from the molecular gearing systems **1**·L₂ under the same conditions because the axial ligands of **1** are easily exchanged.

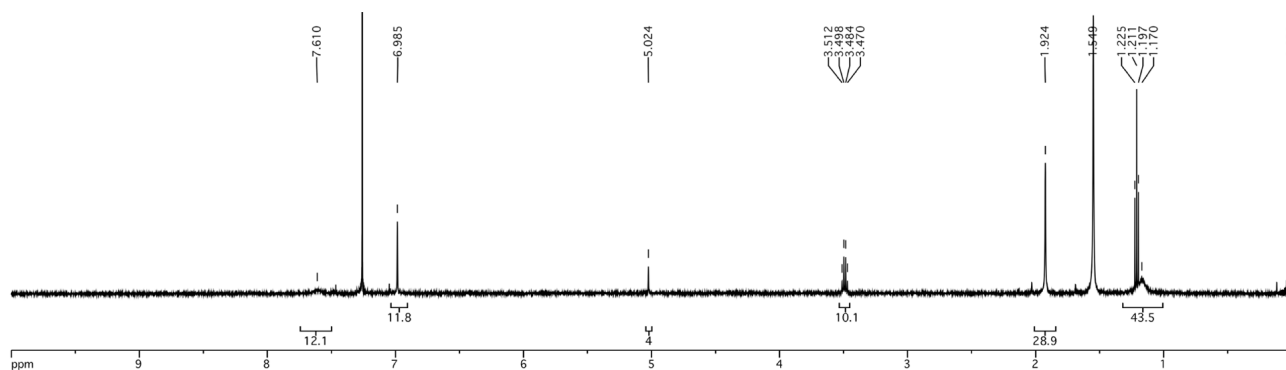


Figure 2-7-19. ¹H NMR spectrum of **1**·(ether)₂ (CDCl₃, 500 MHz, 300 K)

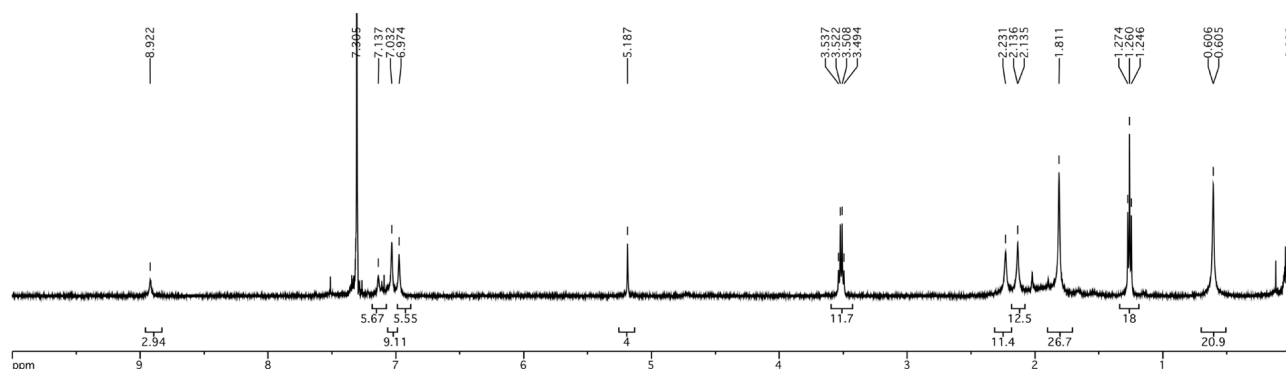
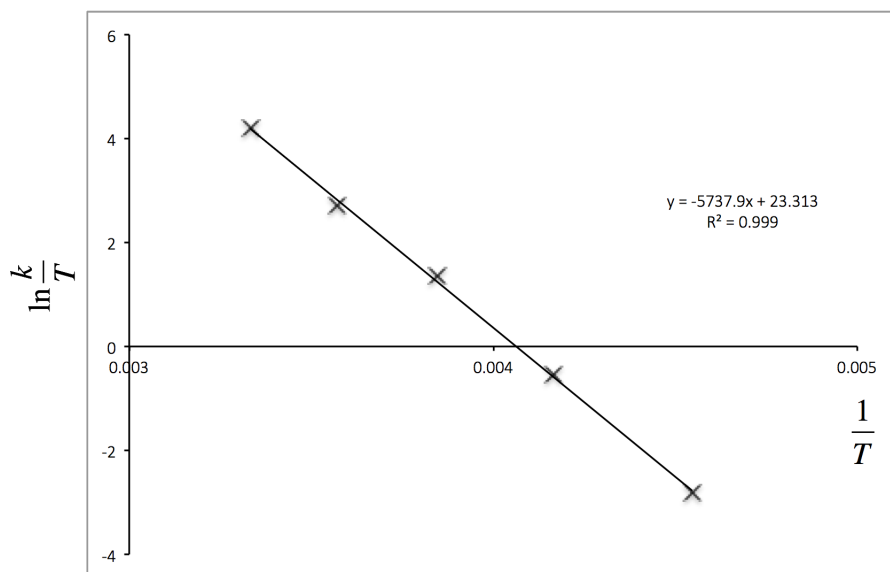


Figure 2-7-20. ¹H NMR spectrum of **1**·(ether)₂ (CDCl₃, 500 MHz, 220 K)



$\Delta G^\ddagger = 11.4 \pm 0.2$ [kcal mol⁻¹], $\Delta S^\ddagger = -0.8 \pm 0.8$ [kcal mol⁻¹ K⁻¹].

Figure 2-7-21. Eyring plot of **1**·(ether)₂

Single-crystal X-ray analysis of **1**·(ether)₂

Crystal suitable for X-ray analysis was obtained by slow evaporation of an Et₂O solution of **1**.

Crystal data for **1**·(ether)₂: C₁₁₆H₁₂₀O₁₀Rh₂, *Fw* = 1880.03, green, block, 0.20 x 0.20 x 0.15 mm, tetragonal, space group *I4*₁/*a* (#88), *a* = 20.7033(6) Å, *c* = 43.948(2) Å, *V* = 18837.3(9) Å³, *Z* = 8, $\rho_{\text{calcd}} = 1.326$ gcm⁻³, $\mu = 4.117$ cm⁻¹, *T* = 93 K, $\lambda(\text{MoK}\alpha) = 0.71075$ Å, $2\theta_{\text{max}} = 55.0^\circ$, 88138/10783 reflections collected/unique (*R*_{int} = 0.0807), *R*₁ = 0.0508 (*I* > 2σ(*I*)), *wR*₂ = 0.1465 (for all data), GOF = 1.071, largest diff. peak and hole 0.78/-1.04 eÅ⁻³. CCDC Deposit number 1442261.

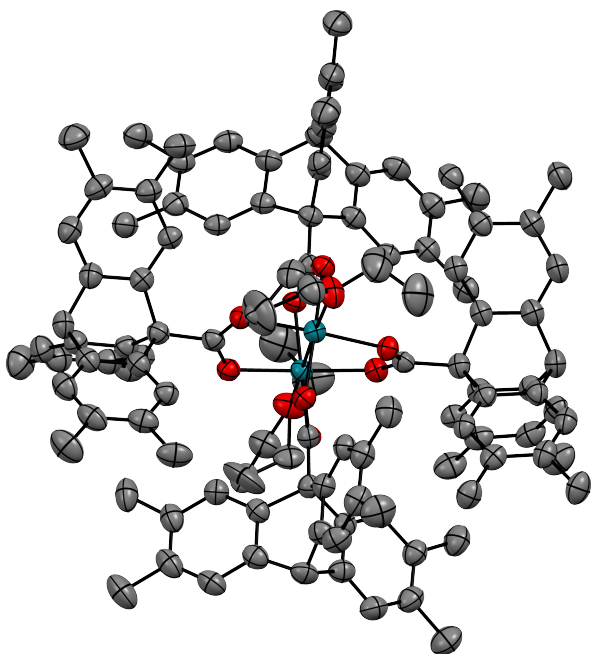


Figure 2-7-22. Crystal structure of **1**·(ether)₂. Thermal ellipsoids set at 50% probability. Color code; C grey, O red, Rh green. Hydrogen atoms in the crystal are omitted for clarity.

Pyridine adduct **1**·(py)₂

A 0.1 M pyridine solution in CH₂Cl₂ (164 μL) was added to a solution of **1**·(Et₂O)_{0.64}(H₂O)_{1.34} (14.8 mg, 8.2 μmol) in CH₂Cl₂ (600 μL) and then evaporated. The solid was recrystallized from vapor diffusion of Et₂O to a CHCl₃ solution, and dried in vacuo to yield **1**·(py)₂·5H₂O as a red solid (3.2 mg, 20%).

¹H NMR (500 MHz; CDCl₃; 300 K): δ 9.88-9.39 (br, 4H), 7.92 (br, 2H), 7.57 (m, 16H), 6.95 (s, 12H), 4.99 (s, 4H), 1.89 (s, 36H), 1.01 (s, 36H); elemental analysis of **1**·(py)₂·5H₂O: Calcd for C₁₁₈H₁₂₀N₂O₁₃Rh₂: C, 71.58; H, 6.11; N, 1.41. Found: C, 71.34; H, 6.01; N, 1.50.

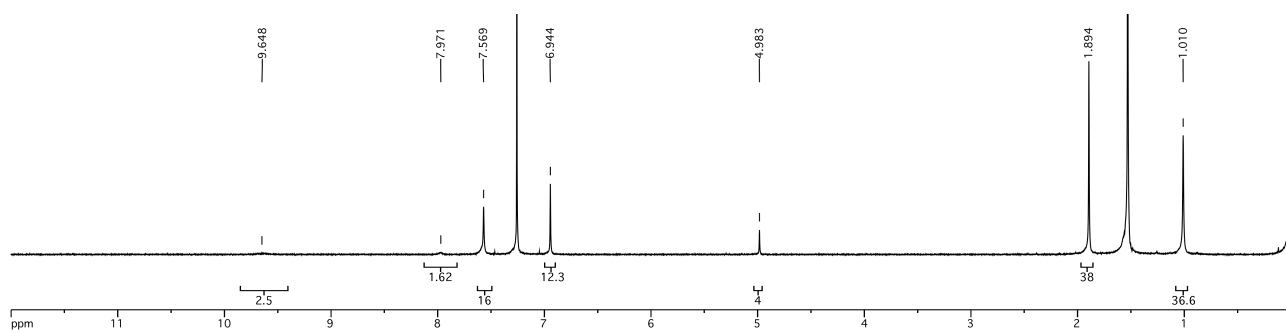


Figure 2-7-23. ^1H NMR spectrum of $\mathbf{1}\cdot(\text{py})_2$ (CDCl_3 , 500 MHz, 300 K)

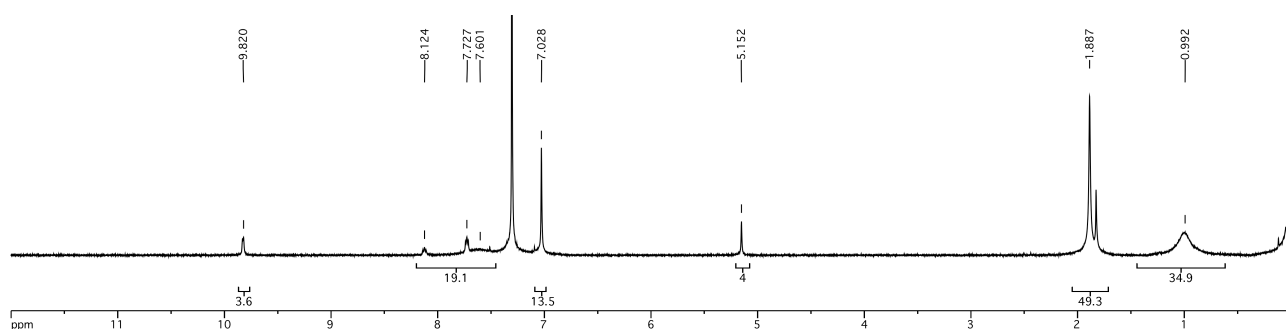


Figure 2-7-24. ^1H NMR spectrum of $\mathbf{1}\cdot(\text{py})_2$ (CDCl_3 , 500 MHz, 220 K)

Single-crystal X-ray analysis of $\mathbf{1}\cdot(\text{py})_2$

Crystal suitable for X-ray analysis was obtained by slow evaporation of an $\text{Et}_2\text{O}/\text{CHCl}_3$ solution of $\mathbf{1}\cdot(\text{py})_2$.

Crystal data for $\mathbf{1}\cdot(\text{py})_2\cdot 2\text{Et}_2\text{O}$: $\text{C}_{126}\text{H}_{130}\text{N}_2\text{O}_{10}\text{Rh}_2$, $F_w = 2038.23$, red, needle, $0.19 \times 0.07 \times 0.06$ mm, orthorhombic, space group $P2_12_12_1$ (#19), $a = 18.3091(5)$ Å, $b = 21.6571(5)$ Å, $c = 27.5325(6)$ Å, $V = 10917.2(5)$ Å³, $Z = 4$, $\rho_{\text{calcd}} = 1.240$ gcm⁻³, $\mu = 3.611$ cm⁻¹, $T = 93$ K, λ (MoK α) = 0.71075 Å, $2\theta_{\text{max}} = 54.9^\circ$, 99867/24851 reflections collected/unique ($R_{\text{int}} = 0.1551$), $R_1 = 0.0777$ ($I > 2\sigma(I)$), $wR_2 = 0.1900$ (for all data), GOF = 1.073, largest diff. peak and hole 1.83/-1.46 eÅ⁻³.
CCDC Deposit number 1442338.

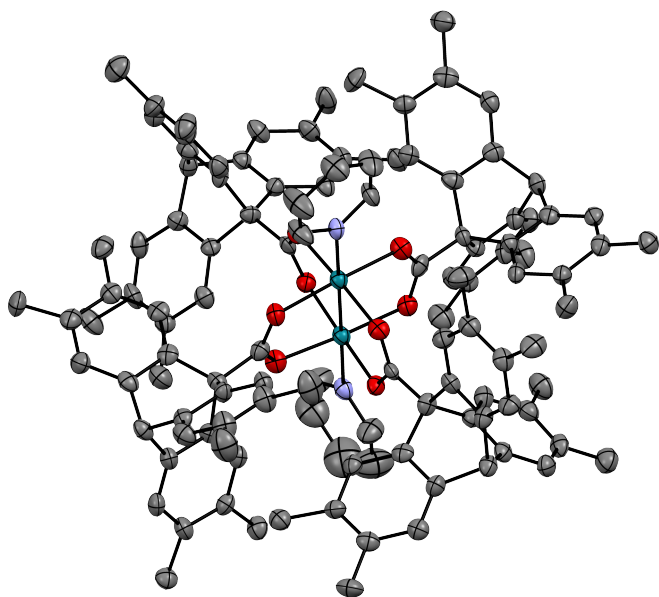


Figure 2-7-25. Crystal structure of **1**·(py)₂. Thermal ellipsoids set at 50% probability. Color code; C grey, N blue, O red, Rh green. Hydrogen atoms in the crystal are omitted for clarity.

2-Methylpyridine adduct **1**·(mepy)₂

A 0.1 M 2-methylpyridine solution in CH₂Cl₂ (168 μL) was added to a solution of **1**·(Et₂O)_{0.64}(H₂O)_{1.34} (15.1 mg, 8.4 μmol) in CH₂Cl₂ (600 μL) and then evaporated. The solid was recrystallized from vapor diffusion of Et₂O and subsequent pentane to CHCl₃ solution, and dried in vacuo to yield **1**·(mepy)₂·1.58C₅H₁₂ as a red solid (12.6 mg, 74%).

¹H NMR (500 MHz; CDCl₃; 300 K): δ 9.50-9.15 (br, 2H), 7.97-7.11 (m, br, 18H), 6.95 (s, 12H), 4.99 (s, 4H), 3.09 (br, 6H), 1.90 (s, 36H), 1.01 (s, 36H); elemental analysis of **1**·(mepy)₂·1.58 C₅H₁₂: Calcd for C_{127.9}H_{132.96}N₂O₈Rh₂: C, 75.60; H, 6.60; N, 1.38. Found: C, 75.27; H, 6.65; N, 1.40.

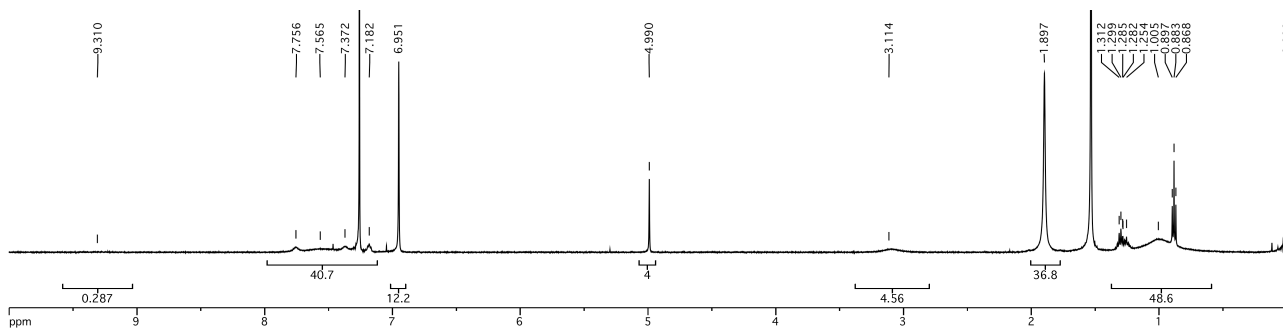


Figure 2-7-26. ^1H NMR spectrum of $\mathbf{1}\cdot(\text{mepy})_2$ (CDCl_3 , 500 MHz, 300 K)

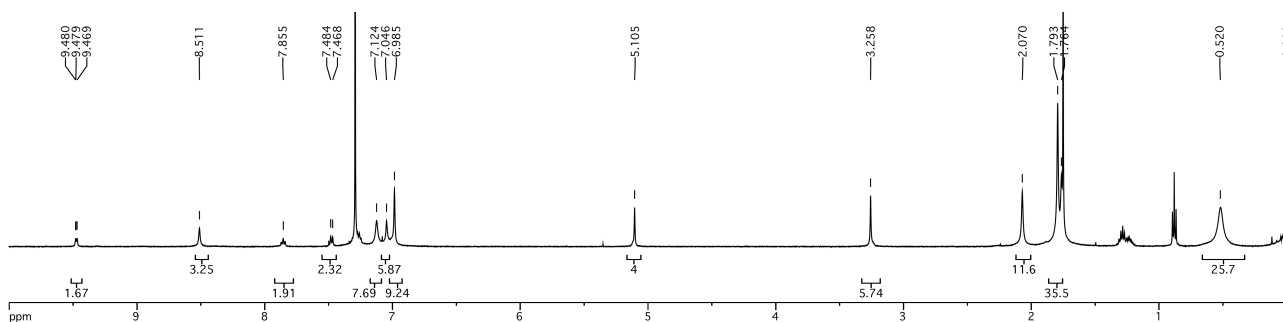


Figure 2-7-27. ^1H NMR spectrum of $\mathbf{1}\cdot(\text{mepy})_2$ (CDCl_3 , 500 MHz, 240 K)

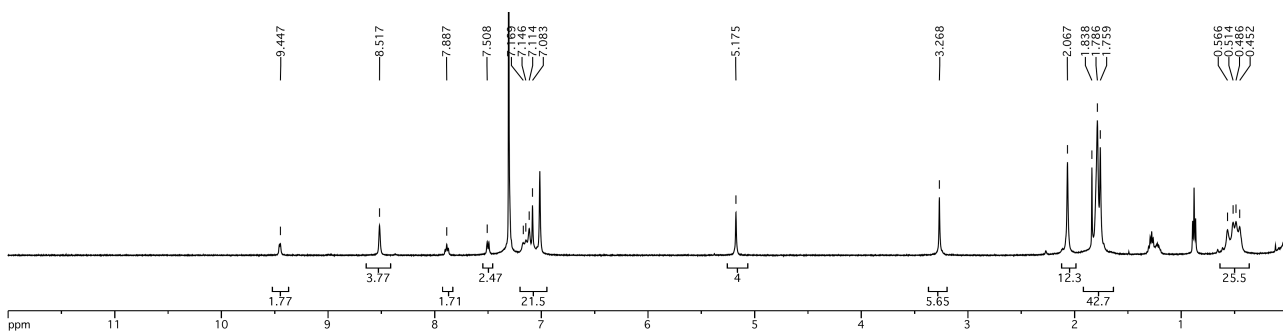
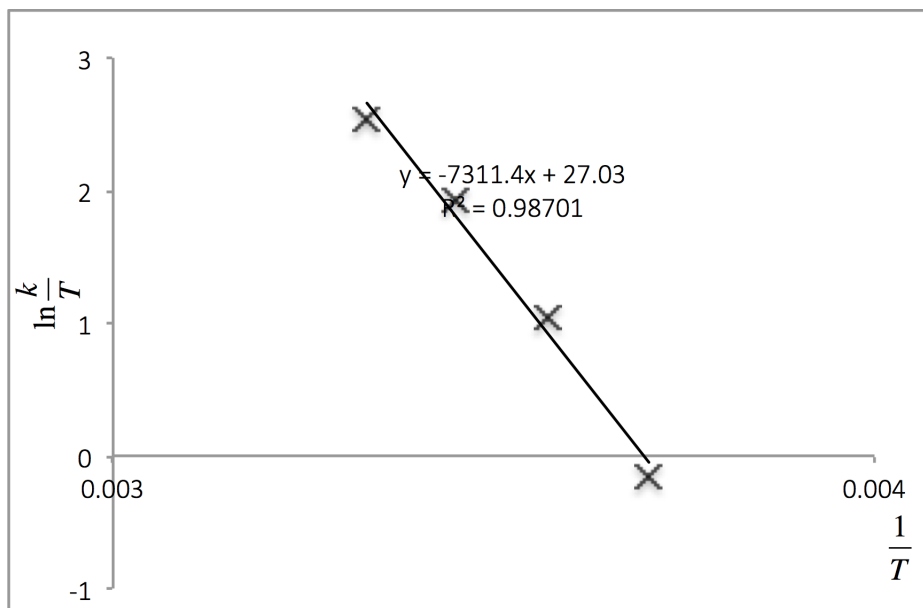


Figure 2-7-28. ^1H NMR spectrum of $\mathbf{1}\cdot(\text{mepy})_2$ (CDCl_3 , 500 MHz, 220 K)



$$\Delta G^\ddagger = 14.5 \pm 1.2 \text{ [kcal mol}^{-1}\text{]}, \Delta S^\ddagger = 6 \pm 4 \text{ [kcal mol}^{-1} \text{ K}^{-1}\text{]}.$$

Figure 2-7-29. Eyring plot of $1 \cdot (\text{mepy})_2$

Single-crystal X-ray analysis of $1 \cdot (\text{mepy})_2$

Crystal suitable for X-ray analysis was obtained by vapor diffusion of pentane to an $\text{Et}_2\text{O}/\text{CH}_2\text{Cl}_2$ solution of $1 \cdot (\text{mepy})_2$.

Crystal data for $1 \cdot (\text{mepy})_2$: $\text{C}_{120}\text{H}_{114}\text{N}_2\text{O}_8\text{Rh}_2$, $F_w = 1918.04$, purple, block, $0.24 \times 0.12 \times 0.06$ mm, monoclinic, space group $C2/c$ (#15), $a = 39.8848(8) \text{ \AA}$, $b = 17.5558(4) \text{ \AA}$, $c = 39.2586(8) \text{ \AA}$, $\beta = 118.6010(7)^\circ$, $V = 24134.8(8) \text{ \AA}^3$, $Z = 10$, $\rho_{\text{calcd}} = 1.320 \text{ g cm}^{-3}$, $\mu = 4.023 \text{ cm}^{-1}$, $T = 93 \text{ K}$, λ (MoK α) = 0.71075 \AA , $2\theta_{\text{max}} = 55.0^\circ$, 112884/27539 reflections collected/unique ($R_{\text{int}} = 0.0807$), $R_1 = 0.0588$ ($I > 2\sigma(I)$), $wR_2 = 0.1868$ (for all data), GOF = 1.111, largest diff. peak and hole $1.57/-1.18 \text{ e\AA}^{-3}$. The contribution of the electron density (836.2 electrons/unit cell) caused by severely disordered molecules in the void ($6555.6 \text{ \AA}^3/\text{unit cell}$) was removed by the SQUEEZE function). CCDC Deposit number 1442269. γ

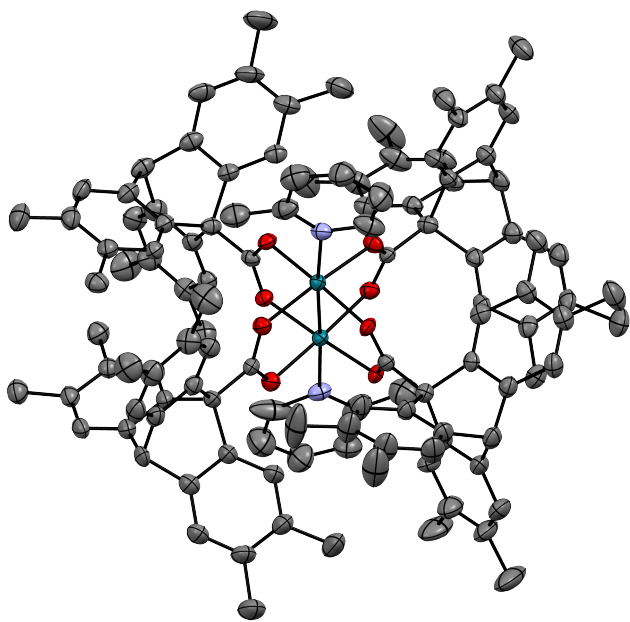


Figure 2-7-30. Crystal structure of **1**·(mepy)₂. Thermal ellipsoids set at 50% probability. Color code; C grey, N blue, O red, Rh green. Hydrogen atoms in the crystal are omitted for clarity.

2-Ethylpyridine adduct **1**·(etpy)₂

A 0.1 M 2-ethylpyridine solution in CH₂Cl₂ (170 μL) was added to a solution of **1**·(Et₂O)_{0.64}(H₂O)_{1.34} (15.3 mg, 8.5 μmol) in CH₂Cl₂ (600 μL) and then evaporated. The solid was recrystallized from vapor diffusion of Et₂O and subsequent pentane to CHCl₃ solution and dried in vacuo to yield **1**·(etpy)₂ as a red solid (8.8 mg, 53%).

¹H NMR (500 MHz; CDCl₃; 300 K): δ 9.50-9.10 (br, 2H), 8.17-7.07 (m, br, 18H), 6.95 (s, 12H), 4.99 (s, 4H), 3.51 (br, 4H), 1.90 (br, 36H), 0.88 (br, 41H); elemental analysis of **1**·(etpy)₂·1.58 C₅H₁₂: Calcd for C₁₂₂H₁₁₈N₂O₈Rh₂: C, 75.30; H, 6.11; N, 1.44. Found: C, 74.91; H, 6.40; N, 1.44.

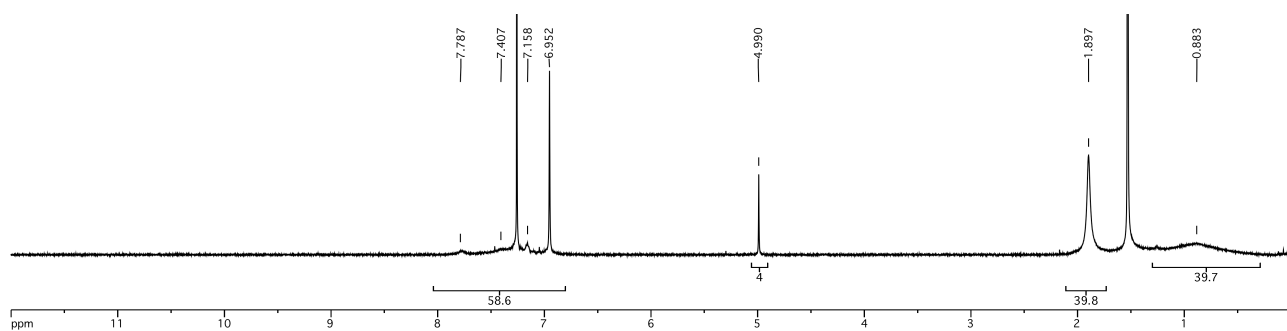


Figure 2-7-31. ^1H NMR spectrum of $\mathbf{1}\cdot(\text{etpy})_2$ (CDCl_3 , 500 MHz, 300 K)

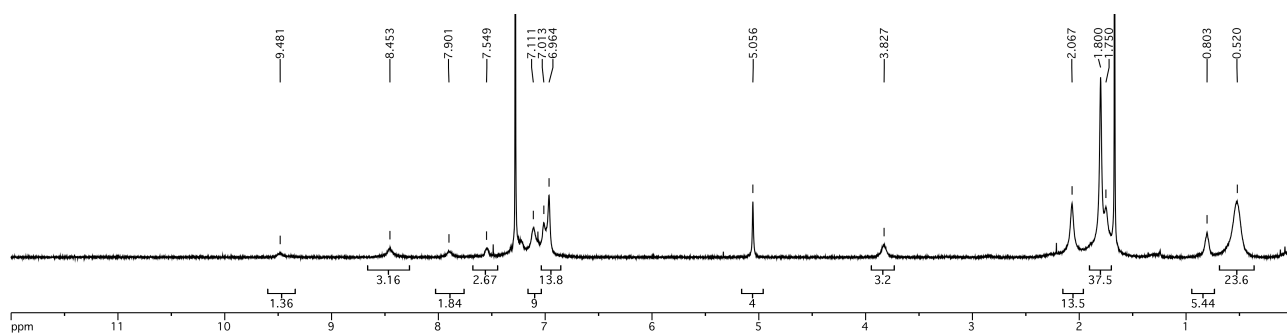


Figure 2-7-32. ^1H NMR spectrum of $\mathbf{1}\cdot(\text{tepy})_2$ (CDCl_3 , 500 MHz, 260 K)

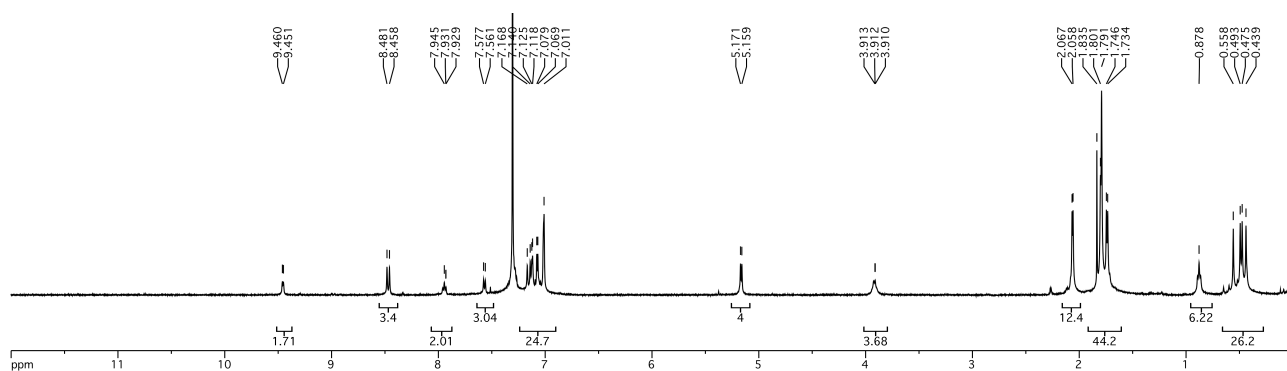
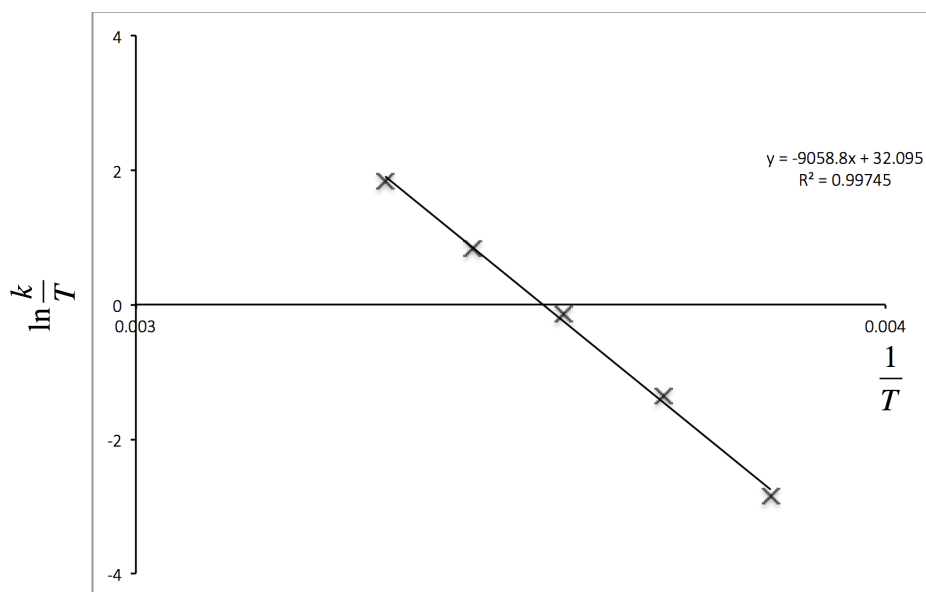


Figure 2-7-33. ^1H NMR spectrum of $\mathbf{1}\cdot(\text{etpy})_2$ (CDCl_3 , 500 MHz, 220 K)



$\Delta G^\ddagger = 18.0 \pm 0.5$ [kcal mol⁻¹], $\Delta S^\ddagger = 16.6 \pm 1.9$ [kcal mol⁻¹ K⁻¹].

Figure 2-7-34. Eyring plot of **1**·(etpy)₂

Single-crystal X-ray analysis of **1**·(etpy)₂

Crystal suitable for X-ray analysis was obtained by vapor diffusion of hexane to an Et₂O/CH₂Cl₂ solution of **1**·(etpy)₂.

Crystal data for **1**·(etpy)₂: C₁₂₂H₁₁₈N₂O₈Rh₂, *F*_w = 1946.09, purple, block, 0.27 x 0.07 x 0.06 mm, triclinic, space group *P*-1 (#2), *a* = 27.1860(5) Å, *b* = 27.8325(5) Å, *c* = 33.4902(6) Å, α = 99.9773(7)°, β = 105.8847(7)°, γ = 117.4669(7)°, *V* = 20250.0(7) Å³, *Z* = 6, ρ_{calcd} = 0.957 gcm⁻³, μ = 2.885 cm⁻¹, *T* = 93 K, λ (MoK α) = 0.71075 Å, $2\theta_{\text{max}}$ = 55.0°, 201921/90027 reflections collected/unique (*R*_{int} = 0.0871), *R*₁ = 0.0735 (*I* > 2σ(*I*)), *wR*₂ = 0.2173 (for all data), GOF = 0.961, largest diff. peak and hole 1.05/-1.62 eÅ⁻³. The contribution of the electron density (1072 electrons/unit cell) caused by severely disordered molecules in the void (7069 Å³/unit cell) was removed by the SQUEEZE function). CCDC Deposit number 1442358.

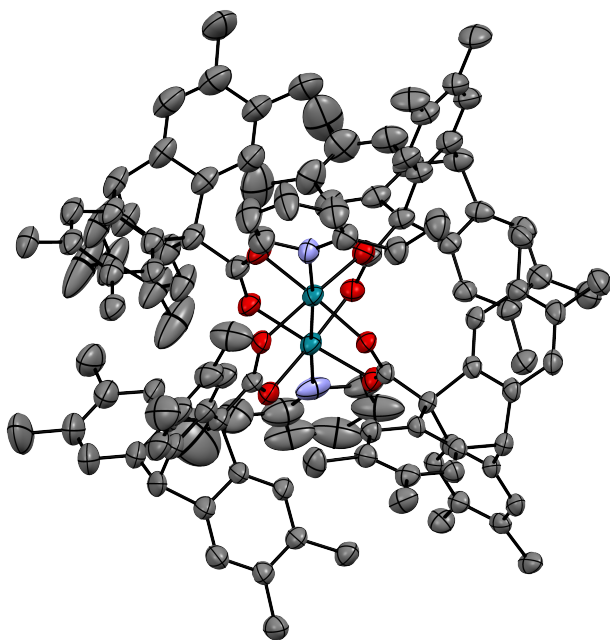


Figure 2-7-35. Crystal structure of **1**·(etpy)₂. Thermal ellipsoids set at 50% probability. Color code; C grey, N blue, O red, Rh green. Hydrogen atoms in the crystal are omitted for clarity.

4-Dimethylaminopyridine adduct **1**·(dmap)₂

A 0.1 M 4-dimethylaminopyridine solution in CH₂Cl₂ (162 μL) was added to a solution of **1**·(Et₂O)_{0.64}(H₂O)_{1.34} (14.7 mg, 8.1 μmol) in CH₂Cl₂ (600 μL) and then evaporated. The solid was recrystallized from vapor diffusion of Et₂O to CHCl₃ solution and dried in vacuo to yield **1**·(dmap)₂ as a red solid (10.6 mg, 66%).

¹H NMR (500 MHz; CDCl₃; 300 K): δ 9.47-9.03 (br, 4H), 7.61 (s, 12H), 6.93 (s, 12H), 6.72 (br, 4H), 4.98 (s, 4H), 3.06 (s, 12H), 1.89 (s, 36H), 1.05 (s, 36H); elemental analysis of **1**·(dmap)₂: Calcd for C₁₂₂H₁₂₀N₂O₈Rh₂: C, 74.15; H, 6.12; N, 2.84. Found: C, 73.91; H, 6.15; N, 2.72.

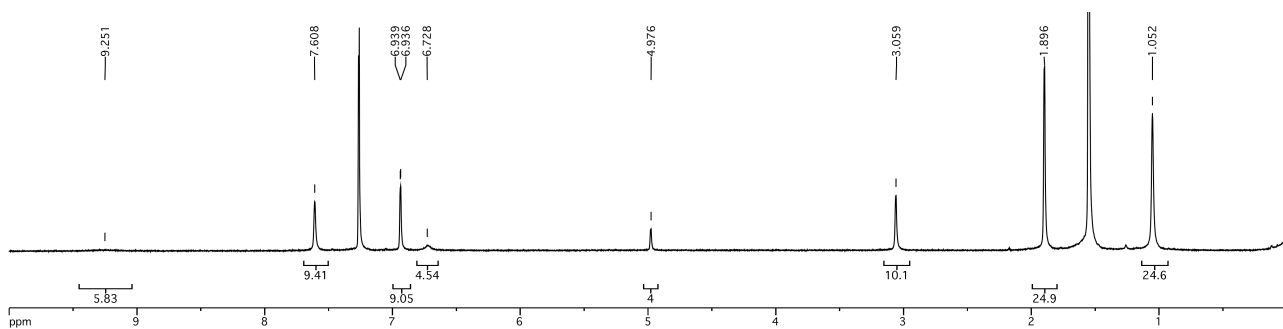


Figure 2-7-36. ^1H NMR spectrum of $\mathbf{1}\cdot(\text{dmap})_2$ (CDCl_3 , 500 MHz, 300 K)

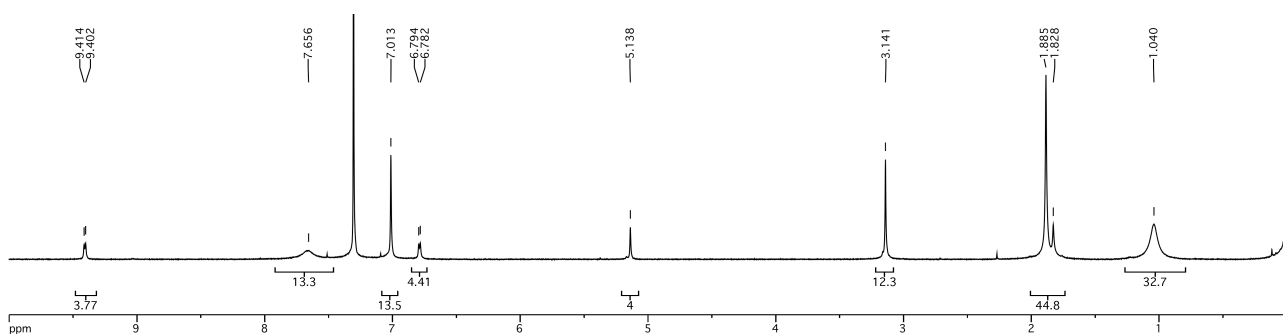


Figure 2-7-37. ^1H NMR spectrum of $\mathbf{1}\cdot(\text{dmap})_2$ (CDCl_3 , 500 MHz, 220 K)

Single-crystal X-ray analysis of $\mathbf{1}\cdot(\text{dmap})_2$

Crystal suitable for X-ray analysis was obtained by vapor diffusion of Et_2O to a CHCl_3 solution of $\mathbf{1}\cdot(\text{dmap})_2$.

Crystal data for $\mathbf{1}\cdot(\text{dmap})_2\cdot\text{Et}_2\text{O}\cdot\text{CHCl}_3$: $\text{C}_{127}\text{H}_{137}\text{Cl}_3\text{N}_4\text{O}_9\text{Rh}_2$, $F_w = 2175.67$, red, block, $0.19 \times 0.12 \times 0.10$ mm, monoclinic, space group $P2_1/c$ (#14), $a = 17.3805(5)$ Å, $b = 25.1289(7)$ Å, $c = 25.2907(8)$ Å, $\beta = 98.6020(8)^\circ$, $V = 10921.5(6)$ Å³, $Z = 4$, $\rho_{\text{calcd}} = 1.323$ gcm⁻³, $\mu = 4.361$ cm⁻¹, $T = 93$ K, λ (MoK α) = 0.71075 Å, $2\theta_{\text{max}} = 55.0^\circ$, 89459/24722 reflections collected/unique ($R_{\text{int}} = 0.1168$), $R_1 = 0.0869$ ($I > 2\sigma(I)$), $wR_2 = 0.2291$ (for all data), GOF = 1.022, largest diff. peak and hole 1.55/-1.42 eÅ⁻³. CCDC Deposit number 1442286.

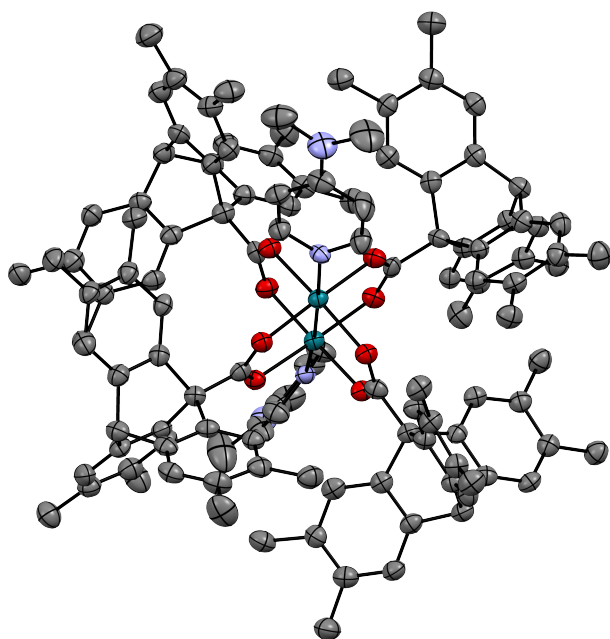


Figure 2-7-38. Crystal structure of **1**·(dmap)₂. Thermal ellipsoids set at 50% probability. Color code; C grey, N blue, O red, Rh green. Hydrogen atoms in the crystal are omitted for clarity.

2-Ethylpyridine adduct **1**·(min)₂

A 0.1 M methyl isonicotinate solution in CH₂Cl₂ (162 μL) was added to a solution of **1**·(Et₂O)_{0.64}(H₂O)_{1.34} (14.6 mg, 8.1 μmol) in CH₂Cl₂ (600 μL) and then evaporated. The solid was recrystallized from vapor diffusion of Et₂O and subsequent pentane to a CHCl₃ solution, and dried in vacuo to yield **1**·(min)₂ as a red solid (14.1 mg, 87%).

¹H NMR (500 MHz; CDCl₃; 300 K): δ 10.01-9.74 (br, 4H), 8.17 (br, 4H), 7.54 (s, 12H), 6.95 (s, 12H), 4.99 (s, 4H), 4.01 (s, 6H), 1.89 (s, 36H), 1.00 (s, 36H); elemental analysis of **1**·(min)₂: Calcd for C₁₂₂H₁₁₄N₂O₁₂Rh₂: C, 73.05; H, 5.73; N, 1.40. Found: C, 72.82; H, 5.81; N, 1.31.

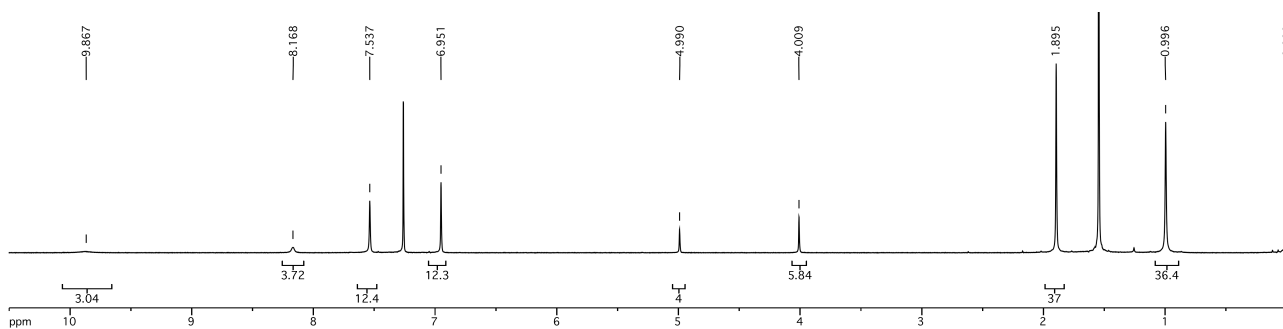


Figure 2-7-39. ^1H NMR spectrum of $\mathbf{1}\cdot(\text{min})_2$ (CDCl_3 , 500 MHz, 300 K)

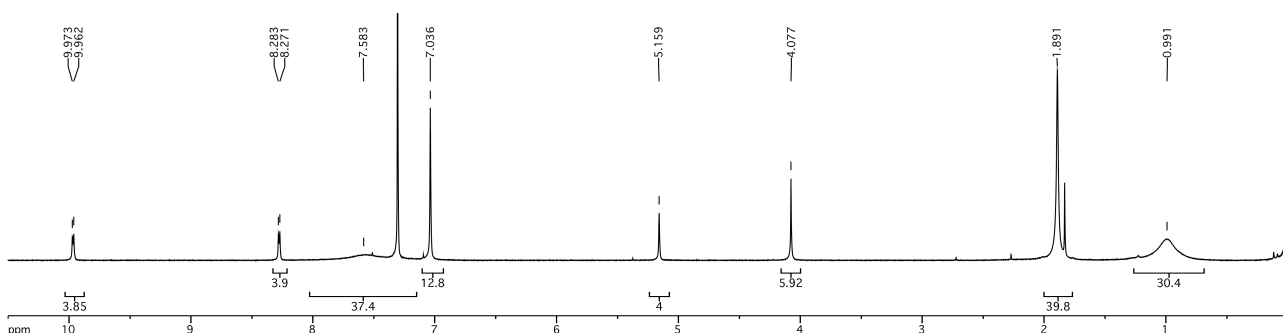


Figure 2-7-40. ^1H NMR spectrum of $\mathbf{1}\cdot(\text{min})_2$ (CDCl_3 , 500 MHz, 220 K)

Single-crystal X-ray analysis of $\mathbf{1}\cdot(\text{min})_2$

Crystal suitable for X-ray analysis was obtained by vapor diffusion of pentane to a CHCl_3 solution of $\mathbf{1}\cdot(\text{min})_2$.

Crystal data for $\mathbf{1}\cdot(\text{min})_2\cdot\text{CH}_2\text{Cl}_2$: $\text{C}_{123}\text{H}_{116}\text{Cl}_2\text{N}_2\text{O}_{12}\text{Rh}_2$, $F_w = 2090.99$, red, block, $0.25 \times 0.21 \times 0.21$ mm, monoclinic, space group $P2_1/n$ (#14), $a = 16.3700(3)$ Å, $b = 32.1927(6)$ Å, $c = 25.1625(5)$ Å, $\beta = 95.3613(7)^\circ$, $V = 13202.5(5)$ Å³, $Z = 6$, $\rho_{\text{calcd}} = 1.578$ gcm⁻³, $\mu = 5.103$ cm⁻¹, $T = 93$ K, λ (MoK α) = 0.71075 Å, $2\theta_{\text{max}} = 54.9^\circ$, 124074/30107 reflections collected/unique ($R_{\text{int}} = 0.0661$), $R_1 = 0.0519$ ($I > 2\sigma(I)$), $wR_2 = 0.1613$ (for all data), GOF = 1.044, largest diff. peak and hole 0.77/-1.17 eÅ⁻³. The contribution of the electron density (140.1 electrons/unit cell) caused by severely disordered molecules in the void (1805.1 Å³/unit cell) was removed by the SQUEEZE

function). CCDC Deposit number 1442359.

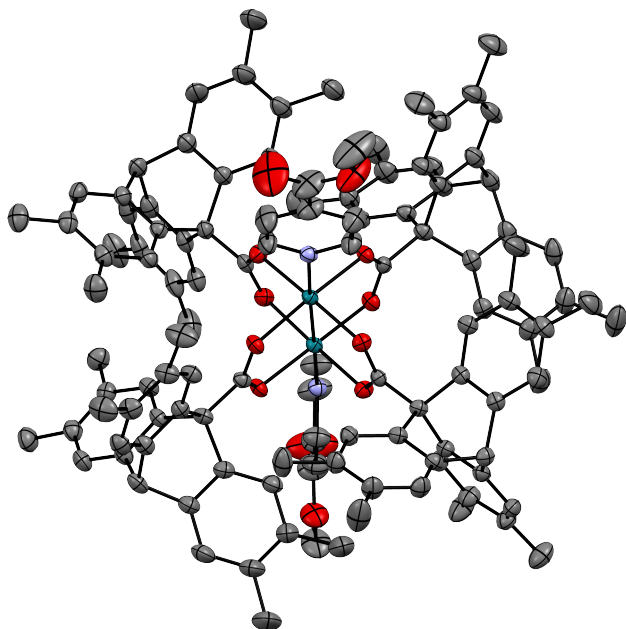


Figure 2-7-41. Crystal structure of $1 \cdot (\text{min})_2$. Thermal ellipsoids set at 50% probability. Color code; C grey, N blue, O red, Rh green. Hydrogen atoms in the crystal are omitted for clarity.

Table 2-7-42. Crystallographic data of **1**·L₂

Complex	1 ·(py) ₂	1 ·(dmap) ₂	1 ·(min) ₂
Formula	C ₁₂₆ H ₁₃₀ N ₂ O ₁₀ Rh ₂	C ₁₂₇ H ₁₃₇ Cl ₃ N ₄ O ₉ Rh ₂	C ₁₂₃ H ₁₁₆ Cl ₂ N ₂ O ₁₂ Rh ₂
Crystal system	orthorhombic	monoclinic	monoclinic
Space group	<i>P</i> 2 ₁ 2 ₁ 2 ₁ (#19)	<i>P</i> 2 ₁ / <i>c</i> (#14)	<i>P</i> 2 ₁ / <i>n</i> (#14)
<i>a</i> /Å	18.3091(5)	17.3805(5)	16.3700(3)
<i>b</i> /Å	21.6571(5)	25.1289(7)	32.1927(6)
<i>c</i> /Å	27.5325(6)	25.2907(8)	25.1625(5)
α /Å	90	90	90
β /Å	90	98.6020(8)	95.3613(7)
γ /Å	90	90	90
<i>V</i> /Å ³	10917.2(5)	10921.5(6)	13202.5(5)
<i>Z</i>	4	4	6
<i>D</i> _{calc} /g cm ⁻³	1.240	1.323	1.578
<i>T</i> /K	93	93	93
μ (Mo-K α)/cm ⁻¹	3.611	4.361	5.103
^a GOF on <i>F</i> ²	1.073	1.022	1.044
^b <i>R</i> 1 [on <i>F</i> , <i>I</i> > 2 σ (<i>I</i>)	0.0777	0.0869	0.0519
^c <i>wR</i> 2 (on <i>F</i> ² , all data)	0.1900	0.2291	0.1613

Complex	1 ·(mepy) ₂	1 ·(etpy) ₂	1 ·(ether) ₂
Formula	C ₁₂₀ H ₁₁₄ N ₂ O ₈ Rh ₂	C ₁₂₂ H ₁₁₈ N ₂ O ₈ Rh ₂	C ₁₁₆ H ₁₂₀ O ₁₀ Rh ₂
Crystal system	monoclinic	triclinic	tetragonal
Space group	<i>C</i> 2/ <i>c</i> (#15)	<i>P</i> -1 (#2)	<i>I</i> 4 ₁ / <i>a</i> (#88)
<i>a</i> /Å	39.8848(8)	27.1860(5)	20.7033(6)
<i>b</i> /Å	17.5558(4)	27.8325(5)	20.7033(6)
<i>c</i> /Å	39.2586(8)	33.4902(6)	43.948(2)
α /Å	90	99.9773(7)	90
β /Å	118.6010(7)	105.8847(7)	90
γ /Å	90	117.4669(7)	90
<i>V</i> /Å ³	24134.8(8)	20250.0(7)	18837.3(9)
<i>Z</i>	10	6	8
<i>D</i> _{calc} /g cm ⁻³	1.320	0.957	1.326
<i>T</i> /K	93	93	93
μ (Mo-K α)/cm ⁻¹	4.023	2.885	4.117
^a GOF on <i>F</i> ²	1.111	0.961	1.071
^b <i>R</i> 1 [on <i>F</i> , <i>I</i> > 2 σ (<i>I</i>)	0.0588	0.0735	0.0508
^c <i>wR</i> 2 (on <i>F</i> ² , all data)	0.1868	0.2173	0.1465

^aGOF = $\{\sum[w(F_o^2 - F_c^2)^2]/(n-p)\}^{1/2}$ (*n*; number of reflections, *p*; total number of parameters refined).

^b*R*1 = $\sum(|F_o| - |F_c|)/\sum|F_o|$, ^c*wR*2 = $\{\sum[w(F_o^2 - F_c^2)^2]/\sum[w(F_o^2)^2]\}^{1/2}$.

2-8. References for Experimental Section

- S1. G. R. Fulmer, A. J. M. Miller, N. H. Sherden, H. E. Gottlieb, A. Nudelman, B. M. Stoltz, J. E. Bercaw, K. I. Goldberg, *Organometallics* **2010**, *29*, 2176–2179.
- S2. G. M. Sheldick, *Acta Crystallogr. Sect. A* **2008**, *64*, 112–122.
- S3. H.-J. Hess, T. H. Cronin, A. Scriabine, *J. Med. Chem.* **1968**, *11*, 130–136.
- S4. M. Gütschow, *J. Org. Chem.* **1999**, *64*, 5109–5115.
- S5. L.-H. Zhang, G. S. Kauffman, J. A. Pesti, J. Yin, *J. Org. Chem.* **1997**, *62*, 6918–6920.
- S6. D. Bender, K. Müllen, *Chem. Ber.* **1988**, *121*, 1187–1197.
- S7. M. Konieczny, R. G. Harvey, *Org. Synth.* **1984**, *62*, 165–169.
- S8. C. E. Godinez, G. Zepeda, C. J. Mortko, H. Dang, M. A. Garcia-Garibay, *J. Org. Chem.* **2004**, *69*, 1652–1662.

3. Conclusions and Perspectives

3-1. Conclusion

In conclusion, I have constructed a circularly-arranged four-gear system based on a lantern-type complex structure with enlarged triptycene gears. The gear system has two axial ligands as control units, and they could be replaced with diethyl ether and five pyridine derivatives and eventually isolated as single crystals.

X-ray crystal analyses revealed that the gear parts are meshed with each other around the lantern-type dinuclear Rh(II) center in all the crystals. Depending on the type of pyridine ligands substituted at the 2-position with proton ($\mathbf{1}\cdot(\text{py})_2$), methyl group ($\mathbf{1}\cdot(\text{mepy})_2$), and ethyl group ($\mathbf{1}\cdot(\text{etpy})_2$), the steric repulsion around the axial ligands was found to remarkably affect the coordination manner. In fact, the coordination distances and angles depend on the bulkiness of the substituents of the pyridine ligands. Their visible absorption spectroscopy demonstrated the apparent color changes of the chloroform solutions. This is mainly due to the bulkiness of the axial ligands. The information about the structure and the motion in solution was obtained by ^1H NMR spectroscopy. The circularly arranged four-gear structure as observed with the crystal structure was evidenced by the upfield shift due to the shielding effect from the adjacent triptycene gears. VT- ^1H NMR experiments further revealed that the rotational rates of triptycene parts of the gearing system depend on the type of the axial ligands.

These results suggested that chemical modification of the triptycene gear would allow the precise control of the rotational rates. The present gearing system would be useful for the control of the motions in molecular machines.

3-2. Perspectives

For future plan, there are three challenging issues that should be investigated: (1) further analysis of the rotational motion, and (2) modularization of the molecular gear system toward higher-functioning molecular machines. (1) Further analysis of the rotational motion: effects of the electronic modification and the type of the donor atoms of axial ligands on the rotational motion should be investigated in detail. The effect of the electronic modification should be demonstrated by X-ray crystal structure analysis and VT-NMR experiments where dmap and min modified by methyl group at the 2-position are used as the axial ligands. Their electronic effect could be clarified by a change of the rotational velocity because the molecular gearing system with 2-methylpyridine rotates slower than the NMR timescale. The effects of the type of the donor atoms on the motion may be examined by similar experiments with *O*-donor ligands (e.g. water and THF) and *S*-donor ligand (e.g. THT). Preliminary VT-NMR experiments suggested some different effects of the type of the donor atoms due to the steric effect on the motion. And slippage rotation should be also investigated. The slippage rotation can be observed from the isomerization of the phase isomers. A gearing system that exhibits the phase isomerism can be synthesized using a new gear molecule that is not C_3 -symmetrical but line-symmetrical, which may be easily synthesized with modified benzyne precursor. Easy observation of the phase isomerism requires a proton peak in a unique region or NMR active nucleus for modification of a blade of the triptycene gear. (2) Modularization of the molecular gear system toward higher-functioning molecular machines: The molecular gear system developed in this study has two expansible points. One is the axial ligand, and the other is the bridge-head position of the triptycene gear. The axial ligand is highly designer,

and a ligand that can be sterically changed by external stimuli would realize the construction of a molecular brake as well as motor of the molecular gear system. The bridge-head position of the triptycene gear will be also useful when it is modified with a ligating substituent or another expansible substituent. These modified molecular gear system will become a higher-functioning molecular machine or a connector unit of other molecular machines (Figure 3-2-1).

The use of the gearing system as a building block of an artificial molecular machine based on these three issues would pioneer a new field different from the biotic approach.

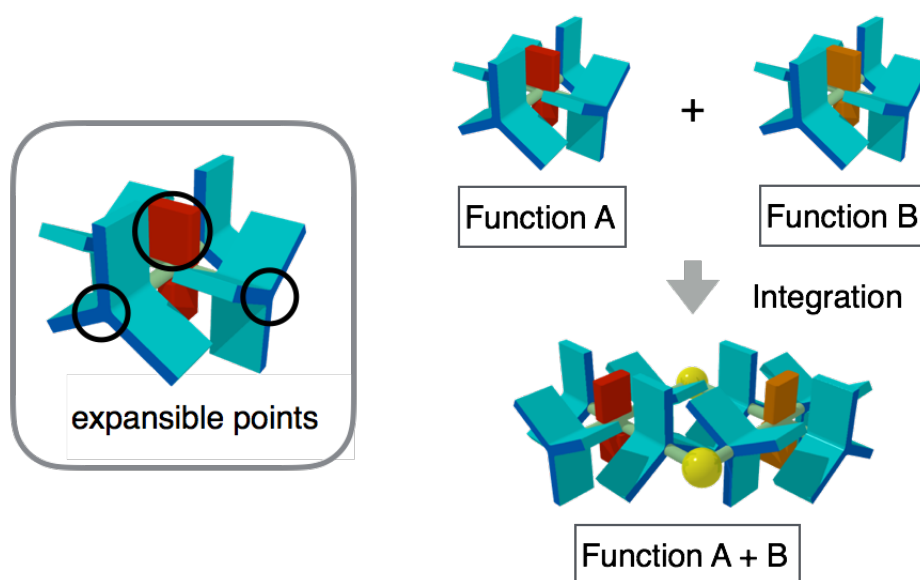


Figure 3-2-1. Modularization using a molecular gear system $1 \cdot L_2$

A List of Publication

[Publication related to the thesis]

1. “Rotational control of a dirhodium-centered circular four-gear system”

Kazuma Sanada, Hitoshi Ube, Mitsuhiko Shionoya.

J. Am. Chem. Soc. **2016**, *138*, 2945-2948.

(corresponding to chapter 2)

Acknowledgement

I would like to express my sincere gratitude to my supervisor, Professor Dr. Mitsuhiko Shionoya (The University of Tokyo), for providing me this precious study opportunity in his laboratory for six years. This study would not have been accomplished without his elaborated guidance, warm encouragement, and invaluable discussion.

I especially would like to express the deepest appreciation to Assistant Professor Dr. Hitoshi Ube (The University of Tokyo), who trained me and discussed with me on a daily basis. Through my six-year study, I have learned many important things such as experimental techniques and logical mind.

I would like to offer my special thanks to Associate Professor Dr. Shohei Tashiro (The University of Tokyo) and Assistant Professor Dr. Yusuke Takezawa (The University of Tokyo) for their kind advise and helpful support to my research in the Bioinorganic Chemistry Laboratory.

I would like to express my gratitude to Ms. Kimiyo Saeki (Systems Engineering Inc.) and Dr. Aiko Kamitsubo (The University of Tokyo) for elemental analysis of the samples.

I would like to thank all the members of the Bioinorganic Chemistry Laboratory. Among them, I appreciate Mr. Yoshihiro Yasuda and Mr. Ryo Yamada for their active discussion in related research about a molecular gearing system.

I owe a very important debt to my family for their everyday support.